fractal and fractional

MDPI

Article

Fractional Reaction–Diffusion Modelling of Immune-Mediated Demyelination in Multiple Sclerosis Under IFN-Beta and Glatiramer Acetate Therapy

Aytekin Enver [1], Fatma Ayaz [1], Mehmet Yavuz [2,3,4,*] and Fuat Usta [5,*]

[1] Department of Mathematics, Gazi University, Ankara 06560, Türkiye; aytekinanwer@gmail.com (A.E.); fayaz@gazi.edu.tr (F.A.)
[2] Department of Mathematics and Computer Sciences, Faculty of Science, Necmettin Erbakan University, Konya 42090, Türkiye
[3] Department of Applied Mathematics and Informatics, Kyrgyz-Turkish Manas University, Bishkek 720038, Kyrgyzstan
[4] Centre for Environmental Mathematics, Faculty of Environment, Science and Economy, University of Exeter, Penryn TR10 9FE, UK
[5] Department of Mathematics, Düzce University, Düzce 81620, Türkiye
* Correspondence: mehmetyavuz@erbakan.edu.tr (M.Y.); fuatusta@duzce.edu.tr (F.U.)

Abstract

We propose a dimensionally consistent fractional spatio-temporal PDE framework for modelling immune-mediated demyelination in multiple sclerosis (MS). The system couples effector and regulatory T cells, M1/M2 macrophage polarisation, pro- and anti-inflammatory cytokines, oligodendrocyte dynamics, and time-dependent therapeutic controls within a unified distributed-parameter structure. In contrast to ad hoc replacements of integer-order derivatives by Caputo fractional derivatives, the fractional extension proposed here is derived from an underlying continuous-time random walk (CTRW) process with Mittag–Leffler-distributed residence times. This stochastic derivation yields a governing system in which a single commensurate fractional order $\alpha \in (0, 1]$, together with a characteristic memory timescale τ_0, ensures dimensional consistency and mass balance across all coupled components. The model is formulated as a system of nonlinear reaction–diffusion equations with cross-regulatory and multiplicative interaction terms governing immune amplification, cytokine feedback, and the demyelination–remyelination balance. Analytical interpretation shows how non-Markovian residence times induce Mittag–Leffler-type relaxation and thereby modify effective growth, decay, and stability properties. Numerical simulations compare classical and fractional dynamics, revealing that memory-driven kinetics prolong effector T-cell and M1-macrophage activity, attenuate reparative M2 and oligodendrocyte responses, and extend the effective action of bang–bang therapy inputs representing IFN-β and glatiramer acetate beyond their dosing windows. The results indicate that integer-order models may underestimate chronic inflammatory persistence and demyelination severity, while providing a mathematically and physically well-posed platform for memory-aware immune modelling and therapy evaluation in MS.

Keywords: fractional reaction–diffusion systems; continuous-time random walk derivation; Mittag–Leffler memory; dimensional consistency; distributed-parameter control

MSC: 35Q92; 92C50; 92C37; 35K57; 65M06

Academic Editor: Bruce Henry

Received: 24 February 2026
Revised: 21 April 2026
Accepted: 22 April 2026
Published: 23 April 2026

1. Introduction

Multiple sclerosis (MS) is a chronic, immune-mediated demyelinating disease of the central nervous system (CNS) [1,2], characterised by multifocal inflammation, loss of oligodendrocytes, and varying degrees of remyelination and axonal damage. Although the pathogenesis of MS involves both adaptive and innate immune responses, therapeutic approaches have largely targeted the modulation of T cell activity and cytokine profiles to delay lesion progression and preserve neurological function. Among the most commonly used first-line therapies are interferon beta (IFN-β) and glatiramer acetate (GA), which exert their effects via modulation of cytokine production, suppression of effector T cells, and enhancement of regulatory T cells and neuroprotective immune phenotypes [3–9].

Multiple sclerosis is characterised by complex interactions between immune activation, inflammatory signalling, and tissue damage within the central nervous system. In particular, effector T cells (T_e) play a central role in driving inflammation, while regulatory T cells (T_r) act to suppress excessive immune responses. Macrophage polarisation further contributes to disease dynamics, with M1 macrophages promoting pro-inflammatory activity and M2 macrophages supporting repair and anti-inflammatory processes. Cytokines, including pro-inflammatory (C_p) and anti-inflammatory (C_a) mediators, regulate communication between immune components and influence both activation and suppression pathways. In addition, oligodendrocytes (O) are responsible for myelin production, and their damage leads to demyelination (D), which is a hallmark of disease progression. The interaction of these variables forms a coupled immune–tissue system, where inflammation, regulation, and repair mechanisms dynamically interact across space and time. The spatio-temporal evolution of the system is illustrated in Figure 1.

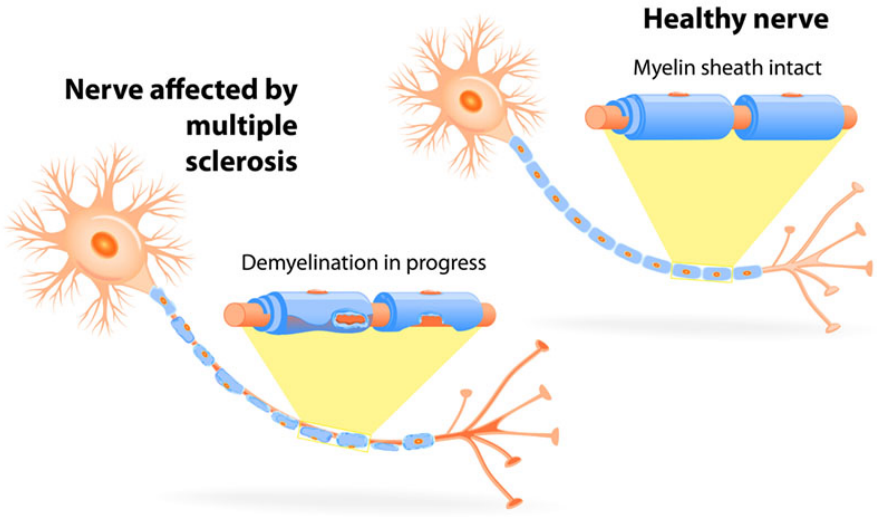

Figure 1. Comparison between a healthy nerve and a nerve affected by multiple sclerosis. The healthy nerve shows an intact myelin sheath, while the MS-affected nerve exhibits demyelination in progress [10].

Reaction–diffusion equations have become one of the most widely used mathematical frameworks for modelling a broad range of diseases and physiological processes in recent years, precisely because they describe the coupled evolution of the relevant biological quantities in both space and time within a single continuum formulation. This combined spatio-temporal resolution, together with the mathematical tractability and mechanistic interpretability of the resulting partial differential equations, has driven a steady growth of reaction–diffusion applications in biomedical modelling, as illustrated for instance in [11–13].

Recent advances in mathematical modelling have provided valuable tools for understanding and simulating the spatio-temporal dynamics of immune responses in MS. However, many existing models focus either on systemic ODE frameworks or on simplified spatial domains that fail to capture the full complexity of MS pathology. For instance, Moise and Friedman [14] proposed a reaction–diffusion PDE model incorporating three spatial domains representing perivascular space, plaque, and normal tissue, where immune cell populations and cytokines were simulated under treatment with IFN-β, GA, and natalizumab [15,16]. Although the model elegantly demonstrated the suppressive effects of therapy on lesion growth, it lacked a mechanistic representation of macrophage polarisation and remyelination processes, which are increasingly recognised as critical in MS progression and repair.

Similarly, de Paula et al. [17] presented a hybrid ODE–PDE model linking peripheral T cell dynamics with CNS innate immune activation, emphasising the bidirectional feedback between adaptive and innate arms of immunity. While this model captured some aspects of effector-regulatory balance, it was limited to a small number of immune variables and did not explicitly model therapeutic effects or macrophage heterogeneity.

Another recent study by Bazlyankov and Ivanov [18] extended a classic reaction–diffusion MS model by introducing a time-delayed remyelination term, thereby allowing the simulation of lesion shrinkage and partial recovery in certain conditions. Yet, this model also neglected adaptive immune mechanisms and cytokine interactions. Finally, the work of Gargano et al. [4] analysed spatial instabilities in cytokine-driven macrophage activation but did not include any therapeutic components or regulatory T cell dynamics.

Despite these advancements, there remains a need for a unified, comprehensive spatial model that (i) integrates both innate and adaptive immune responses, (ii) accounts for phenotypic switching of macrophages (M1 $\leftrightarrow$ M2), (iii) models pro- and anti-inflammatory cytokine dynamics, and (iv) includes distinct and combined therapeutic effects of IFN-β and GA on the immune network.

In recent years, fractional-order models have gained increasing attention in biomedical applications due to their ability to capture memory and hereditary effects that are not represented in classical integer-order systems [19–21]. Biological processes such as immune response, inflammation, and tissue repair are inherently history-dependent, meaning that their current state is influenced not only by present conditions but also by past interactions. In particular, chronic diseases such as multiple sclerosis exhibit long-term immune activation, delayed regulatory responses, and persistent inflammatory feedback, which cannot be adequately described using Markovian dynamics. Fractional derivatives, especially in the Caputo sense, provide a mathematically consistent framework for incorporating such nonlocal temporal effects through power-law memory kernels. This enables the modelling of slow relaxation, cumulative activation, and sustained immune persistence, which are key features of neuroinflammatory processes. Therefore, the use of fractional reaction–diffusion models offers a more realistic and flexible approach for representing the complex temporal dynamics of immune-mediated diseases compared to classical integer-order formulations [22–25].

Contribution of This Study

This study develops a fractional spatio-temporal reaction–diffusion framework for modelling lesion dynamics in multiple sclerosis (MS), with emphasis on capturing the interplay between immune regulation, inflammatory signalling, and tissue damage within a spatially distributed setting. The model integrates the key biological components effector T cells (Th1/Th17), regulatory T cells (Treg), macrophage polarisation (M1/M2), cytokine-

mediated feedback, and oligodendrocyte dynamics within a unified representation of the adaptive and innate immune response.

The governing system is formulated as a set of coupled nonlinear partial differential equations incorporating spatial diffusion, nonlinear reaction kinetics, and time-dependent therapeutic control functions representing IFN-β and glatiramer acetate. This structure enables the systematic investigation of treatment timing, dosage, and interaction with immune dynamics in a mechanistically interpretable manner.

A central methodological feature of the present framework is that the fractional extension of the classical model is not obtained by ad hoc replacement of integer-order time derivatives with Caputo fractional derivatives. Such a substitution, while widely adopted in the literature, has been shown to be problematic in several respects for coupled reaction–diffusion systems: it can violate dimensional consistency, break mass conservation, and yield unphysical solutions [26,27]. Moreover, assigning heterogeneous fractional orders to different coupled compartments, as in an earlier component-wise fractional memory formulation, generally cannot be reconciled with the dimensional balance of shared interaction terms [27].

To resolve these difficulties, the fractional model proposed here is derived from an underlying continuous-time random walk (CTRW) process with Mittag–Leffler-distributed residence times, following the physically consistent construction developed by Angstmann, Henry and co-workers. This yields a commensurate fractional system, in which a single memory order $\alpha \in (0, 1]$ and a characteristic timescale τ_0 enter the governing equations through a natural dimensional prefactor τ_0^α. The resulting model is dimensionally consistent, preserves mass balance, and reduces to the classical integer-order formulation in the Markovian limit $\alpha \to 1$.

From a mathematical perspective, the model is supported by rigorous analysis of existence, uniqueness, positivity, boundedness, and well-posedness of solutions, together with a stability analysis of equilibrium states. These results ensure that the proposed system is both mathematically consistent and biologically admissible.

Numerical simulations are carried out to compare the classical integer-order and dimensionally consistent fractional dynamics. The results highlight qualitative differences in lesion persistence, inflammatory amplification, and recovery, attributable to the non-Markovian residence-time distribution rather than to an increase in effective reaction rates. In this sense, the fractional formulation is not intended to quantitatively outperform the classical model, but to provide a mechanistic extension that captures memory-driven dynamics arising from prolonged immune activation.

The primary contribution of this work therefore lies in the structured integration of established reaction–diffusion modelling of MS, a CTRW-based stochastic derivation of the fractional operator, and therapy-dependent dynamics within a single, biologically motivated, dimensionally consistent framework. This integrated formulation enables the systematic investigation of how immune memory influences amplification, persistence, and treatment response in MS, thereby providing mechanistic insights that are not accessible through classical formulations or ad hoc fractional replacements considered in isolation. The contributions are thus primarily structural and interpretative, providing a flexible in silico platform for analysing immune-driven lesion evolution and supporting future developments involving parameter calibration, sensitivity analysis, and integration with clinical or imaging data.

2. Mathematical Model

In this section we formulate the spatio-temporal reaction–diffusion model governing multiple sclerosis (MS) lesion dynamics under therapeutic modulation by interferon beta

(IFN-β) and glatiramer acetate (GA). The model is formulated as a nonlinear system of coupled partial differential equations, with a single fractional temporal operator of commensurate Caputo order $\alpha \in (0, 1]$ and a characteristic memory timescale τ_0, derived in Section 2.4 from an underlying continuous-time random walk (CTRW) process. The classical integer-order system is recovered as the Markovian limit $\alpha \to 1$, $\tau_0 \to 1$ day.

The formulation captures the multiscale interplay between adaptive and innate immune responses, cytokine-mediated feedback regulation, macrophage phenotypic polarisation, and the demyelination–remyelination balance of oligodendrocytes. Spatial propagation is represented by diffusion operators on a bounded domain, whereas nonlinear reaction terms describe immune activation, cross-regulatory suppression, and tissue damage mechanisms.

Let $\Omega \subset \mathbb{R}^n$, $n \in \{1, 2, 3\}$, be a bounded domain with sufficiently smooth boundary $\partial\Omega$, and let $t \in [0, T]$ denote time. The state of the system is described by the eight-component vector

$$U(x,t) = \left(T_e,\, T_r,\, M_1,\, M_2,\, C_p,\, C_a,\, O,\, D\right)^\top : \overline{\Omega} \times [0,T] \to \mathbb{R}^8_+. \tag{1}$$

where $T_e(x,t)$ and $T_r(x,t)$ denote the densities of effector (Th1/Th17) and regulatory (Treg) T cells respectively; $M_1(x,t)$ and $M_2(x,t)$ denote the densities of classically activated pro-inflammatory macrophages and alternatively activated anti-inflammatory macrophages; $C_p(x,t)$ and $C_a(x,t)$ denote the concentrations of pro-inflammatory cytokines (such as IFN-γ and IL-17) and anti-inflammatory cytokines (such as IL-10); $O(x,t)$ denotes healthy oligodendrocyte density; and $D(x,t)$ denotes the demyelinated lesion volume. Each component is required to be non-negative and bounded, i.e., $\mathbf{U}(\cdot,t) \in L^\infty(\Omega)^8$ for every $t \in [0,T]$; these requirements are established rigorously in Section 3.

Therapeutic interventions are modelled through time-dependent control inputs

$$\Phi_1, \Phi_2 \;:\; [0,T] \longrightarrow \mathbb{R}_{\geq 0}, \tag{2}$$

where $\Phi_1(t)$ denotes IFN-β intensity and $\Phi_2(t)$ denotes GA intensity. These functions act multiplicatively on selected immune and cytokine subsystems, so that the fully controlled governing system may be written in the abstract form

$${}^{C}\mathcal{D}^{\alpha}_{t}\, U(x,t) = \tau_0^{\alpha}\Big[\mathcal{D}\,\Delta U(x,t) + F\big(U(x,t),\, \Phi_1(t),\, \Phi_2(t)\big)\Big], \qquad (x,t) \in \Omega \times (0,T], \tag{3}$$

subject to homogeneous Neumann boundary conditions $\partial_n \mathbf{U}\big|_{\partial\Omega} = 0$ and to non-negative initial data $\mathbf{U}(x,0) = \mathbf{U}_0(x) \geq 0$. Here, $\mathcal{D} = \mathrm{diag}(D_T, D_T, D_M, D_M, D_C, D_C, 0, 0)$ is the component-wise diffusion matrix, Δ is the spatial Laplacian, and $\mathbf{F}$ collects the nonlinear reaction, cross-regulation, and therapy terms.

The explicit componentwise form of (3) is presented below, first in the classical integer-order setting and subsequently in its dimensionally consistent fractional extension obtained from the CTRW derivation of Section 2.4. This structured state-space representation enables systematic investigation of immune amplification, regulatory compensation, macrophage polarisation shifts, and therapy-induced modulation within a unified distributed-parameter framework.

2.1. Governing Equations

The evolution of the immune and tissue components is governed by the following nonlinear reaction–diffusion system:

Effector T cells (Th1/Th17):

$$\frac{\partial T_e}{\partial t} = D_T \nabla^2 T_e + \kappa_e C_p - \delta_e T_e - \gamma_1 T_r T_e - \xi_1 \Phi_2(t) T_e. \tag{4}$$

Regulatory T cells (Treg):

$$\frac{\partial T_r}{\partial t} = D_T \nabla^2 T_r + \kappa_r C_a - \delta_r T_r + \xi_2 \Phi_2(t). \tag{5}$$

M1 macrophages (pro-inflammatory):

$$\frac{\partial M_1}{\partial t} = D_M \nabla^2 M_1 + \beta_1 C_p - \delta_{M_1} M_1 - \gamma_2 M_2 M_1 - \xi_3 \Phi_1(t) M_1. \tag{6}$$

M2 macrophages (anti-inflammatory):

$$\frac{\partial M_2}{\partial t} = D_M \nabla^2 M_2 + \beta_2 C_a - \delta_{M_2} M_2 + \xi_4 \Phi_1(t). \tag{7}$$

Pro-inflammatory cytokines:

$$\frac{\partial C_p}{\partial t} = D_C \nabla^2 C_p + \eta_1 T_e + \eta_2 M_1 - \mu_p C_p - \xi_5 \Phi_1(t) C_p. \tag{8}$$

Anti-inflammatory cytokines:

$$\frac{\partial C_a}{\partial t} = D_C \nabla^2 C_a + \zeta_1 T_r + \zeta_2 M_2 - \mu_a C_a + \xi_6 \Phi_1(t) + \xi_7 \Phi_2(t). \tag{9}$$

Healthy oligodendrocytes:

$$\frac{\partial O}{\partial t} = -\lambda_1 C_p O + \lambda_2 M_2 - \delta_O O. \tag{10}$$

Demyelinated area:

$$\frac{\partial D}{\partial t} = \lambda_1 C_p O - \lambda_2 M_2. \tag{11}$$

The system (4)–(11) constitutes the classical integer-order formulation of the MS lesion dynamics. To incorporate the non-Markovian persistence of immune activation that is characteristic of chronic neuroinflammatory processes, we extend this system by replacing the first-order time derivatives with a single commensurate Caputo fractional derivative of order $\alpha \in (0, 1]$. The resulting fractional formulation is not obtained by direct ad hoc substitution but is derived in Section 2.4 from an underlying continuous-time random walk (CTRW) process with Mittag–Leffler-distributed residence times. This derivation yields a dimensionally consistent and mass-conserving system in which each equation assumes the general form

$${}^{C}\mathcal{D}_t^{\alpha} u(x,t) = \tau_0^{\alpha} \Big[D_u \nabla^2 u + \mathcal{R}_u(\mathbf{U}, \Phi_1, \Phi_2) \Big], \qquad 0 < \alpha \leq 1, \tag{12}$$

where the Caputo fractional derivative is defined by

$${}^{C}\mathcal{D}_t^{\alpha} u(t) = \frac{1}{\Gamma(1-\alpha)} \int_0^t \frac{\partial u(\tau)}{\partial \tau} (t-\tau)^{-\alpha} \, d\tau, \tag{13}$$

and the prefactor τ_0^α (of dimension day$^\alpha$) ensures that both sides of (12) share the common dimension $[u] \cdot \text{day}^{-\alpha}$. The classical integer-order system (4)–(11) is recovered as the Markovian limit $\alpha \to 1$, $\tau_0 \to 1$ day. The componentwise fractional system obtained from this construction is given explicitly in Section 2.5.

2.2. Therapy Functions

The therapy controls $\Phi_1(t)$ and $\Phi_2(t)$ are modelled as bounded piecewise-constant inputs,

$$\Phi_1(t) = \chi_1 \mathbf{1}_{[t_1,t_2]}(t), \qquad \Phi_2(t) = \chi_2 \mathbf{1}_{[t_3,t_4]}(t), \tag{14}$$

where $\chi_1, \chi_2 \geq 0$ are the therapy intensities and $\mathbf{1}_{[a,b]}(t)$ denotes the indicator function of the interval $[a, b]$. In the integer-order system, these controls act instantaneously on the associated reaction terms and vanish as soon as they are switched off. In the fractional system, the controls remain multiplicative but are convolved against the Mittag–Leffler kernel inherited from the CTRW derivation; consequently, their influence persists beyond the nominal dosing window with an algebraic rather than exponential decay profile.

2.3. Initial and Boundary Conditions

Homogeneous Neumann (zero-flux) boundary conditions are imposed on every component of the state vector:

$$\left.\frac{\partial u}{\partial \mathbf{n}}\right|_{\partial\Omega} = 0, \qquad \forall\, u \in \{T_e, T_r, M_1, M_2, C_p, C_a, O, D\}. \tag{15}$$

These conditions preserve the spatial integral of each component under pure diffusion and exclude artificial boundary flux.

Initial data are prescribed as non-negative spatial profiles,

$$\begin{aligned} &T_e(x,0) = T_{e0}(x), \quad T_r(x,0) = T_{r0}(x), \quad M_1(x,0) = M_{10}(x), \quad M_2(x,0) = M_{20}(x), \\ &C_p(x,0) = 0, \quad C_a(x,0) = 0, \quad O(x,0) = O_0(x), \quad D(x,0) = 0, \end{aligned} \tag{16}$$

with $T_{e0}, T_{r0}, M_{10}, M_{20}, O_0 \in L^\infty(\Omega)$ and $T_{e0}, T_{r0}, M_{10}, M_{20}, O_0 \geq 0$. The vanishing initial cytokine concentrations reflect the modelling assumption that soluble mediators accumulate only once cellular activation has begun, while $D(x, 0) = 0$ corresponds to the absence of demyelinated tissue at the onset of the simulation.

The formulation presented in this section captures bidirectional immune–cytokine coupling, spatially resolved inflammatory propagation, demyelination–remyelination balance, and therapy modulation within a unified distributed-parameter framework. Its dimensionally consistent fractional extension, derived in Section 2.4 and presented explicitly in Section 2.5, enables a systematic investigation of memory-driven activation, regulatory retardation, and long-term lesion evolution.

2.4. Stochastic Derivation of the Fractional Model via Continuous-Time Random Walks

A critical issue in formulating fractional reaction–diffusion systems for biological processes is that replacing integer-order time derivatives with Caputo fractional derivatives in an ad hoc manner may violate mass balance, break dimensional consistency, and yield unphysical solutions [26,27]. In particular, when different compartments are assigned different fractional orders, the resulting coupled system generally cannot be made dimensionally consistent unless the fractional orders coincide [27]. To overcome these difficulties, we derive the fractional extension of the MS model directly from an underlying stochastic process, following the continuous-time random walk (CTRW) framework developed by Angstmann,

Henry and co-workers [26–28]. This ensures that the resulting governing equations are physically motivated, dimensionally consistent, and mass-conserving by construction.

2.4.1. Non-Markovian Waiting Times for Immune Populations

Let $u(x,t)$ denote the density of a generic immune or tissue population (such as T_e, T_r, M_1, M_2, C_p, C_a, O, or D). In the classical (Markovian) description, the time a particle spends in its current state before being removed (through death, deactivation, differentiation, or clearance) follows an exponential distribution with constant rate δ, leading to an integer-order decay term $-\delta u$.

In chronic immune-mediated diseases such as multiple sclerosis, however, activated effector cells, polarised macrophages, and inflammatory cytokines exhibit persistent, non-Markovian residence in their activated state, consistent with extended lifetimes and cumulative activation effects [4,14]. To capture this, we assume that the residence time τ of an arbitrary particle in its current state is drawn from a Mittag–Leffler distribution with survival function

$$\Phi_\alpha(t) \;=\; E_\alpha\Big(-\Big(\tfrac{t}{\tau_0}\Big)^\alpha\Big), \qquad 0<\alpha\le 1, \tag{17}$$

where $\tau_0 > 0$ is a characteristic time scale (with physical dimension of time, $[\tau_0] = T$) and $E_\alpha(\cdot)$ is the single-parameter Mittag–Leffler function. The limit $\alpha \to 1$ recovers the exponential survival function $\Phi_1(t) = e^{-t/\tau_0}$ of the Markovian model, whereas $\alpha < 1$ produces a heavy-tailed, power-law decay, $\Phi_\alpha(t) \sim t^{-\alpha}/\Gamma(1-\alpha)$ as $t \to \infty$. This heavy-tailed behaviour encodes the cumulative, history-dependent persistence of immune activation that is characteristic of progressive MS.

The associated waiting-time probability density function is

$$\psi_\alpha(t) \;=\; -\frac{d\Phi_\alpha(t)}{dt} \;=\; \frac{1}{\tau_0}\Big(\tfrac{t}{\tau_0}\Big)^{\alpha-1} E_{\alpha,\alpha}\Big(-\big(\tfrac{t}{\tau_0}\big)^\alpha\Big), \tag{18}$$

where $E_{\alpha,\alpha}$ is the two-parameter Mittag–Leffler function.

2.4.2. Master Equation and Continuum Limit

Consider the density $u(x,t)$ evolving under (i) diffusive spatial transport with diffusivity D_u, (ii) production at rate $S(x,t)$ (which may itself depend on other state variables), and (iii) removal governed by the Mittag–Leffler survival function (17). Following the CTRW formalism of [26,27], the probability conservation equation for the density reads

$$u(x,t) \;=\; \int_0^t q(x,t')\,\Phi_\alpha(t-t')\,dt' \;+\; u_0(x)\,\Phi_\alpha(t), \tag{19}$$

where $q(x,t)$ is the arrival density of newly produced particles at (x,t), and $u_0(x) = u(x,0)$. Equation (19) states that the density at time t equals the fraction of particles that were produced earlier and have not yet been removed, plus the fraction of initial particles that still survive.

Taking the Laplace transform of (19), using the identity $\mathcal{L}\{\Phi_\alpha\}(s) = \tau_0^\alpha\, s^{\alpha-1}/(1+\tau_0^\alpha s^\alpha)$, and combining with the balance equation

$$q(x,t) \;=\; D_u\,\Delta u(x,t) \;+\; S(x,t), \tag{20}$$

we obtain, after inverse Laplace transformation, the governing equation

$$\frac{\partial u(x,t)}{\partial t} = \tau_0^{\alpha-1}\,{}_0\mathcal{D}_t^{1-\alpha}\Big[\,D_u\,\Delta u(x,t) + S(x,t)\,\Big] - \frac{1}{\tau_0^\alpha}\,{}_0\mathcal{D}_t^{1-\alpha}\,u(x,t), \tag{21}$$

where ${}_0\mathcal{D}_t^{1-\alpha}$ denotes the Riemann–Liouville fractional derivative of order $1-\alpha$.

Equivalently, (21) admits the Caputo formulation

$$ {}^{C}\mathcal{D}_t^{\alpha}\, u(x,t) \;=\; \tau_0^{\alpha}\Big[\, D_u\, \Delta u(x,t)\,\Big] \;-\; u(x,t) \;+\; \tau_0^{\alpha}\, S(x,t), \qquad 0<\alpha\le 1, \tag{22} $$

which makes explicit the role of τ_0^{α} as the dimensional bridge between fractional and classical kinetics. Crucially, both sides of (22) have the correct physical dimensions $[u]\cdot T^{-\alpha}$, because the factor τ_0^{α} (of dimension T^{α}) multiplies all reaction-rate and diffusion terms whose natural dimension is $[u]\cdot T^{-1}$.

Remark 1 (Dimensional consistency)**.** *Equation* (22) *is dimensionally consistent for all admissible* $\alpha\in(0,1]$*. The intrinsic time scale* τ_0 *inherited from the Mittag–Leffler waiting-time distribution absorbs the dimensional mismatch introduced by the fractional operator. In contrast, the naive ad hoc substitution* $\partial_t u \mapsto {}^{C}\mathcal{D}_t^{\alpha}u$ *without rescaling leads to inconsistent dimensions whenever* $\alpha\neq 1$*, as emphasised in [27].*

Remark 2 (Mass conservation)**.** *Equation* (22) *is derived directly from the probability-conservation identity* (19)*. Therefore, in the absence of sources and sinks (*$S\equiv 0$ *and no removal), the total mass* $\int_\Omega u(x,t)\,dx$ *is conserved under Neumann boundary conditions. This property does not generally hold for ad hoc Caputo replacements in coupled systems with heterogeneous orders [27].*

2.4.3. Constraint on the Fractional Orders

In a coupled multi-component system with shared reaction pathways (e.g., cytokine-mediated activation of effector cells by pro-inflammatory cytokines), the CTRW derivation imposes a compatibility condition: the fractional order α is a global property of the underlying non-Markovian transport process across the coupled immune network [26,27]. Assigning distinct fractional orders $\alpha_i \neq \alpha_j$ to different coupled compartments generically break flux balance and dimensional consistency, because the interaction terms (e.g., $\gamma_1 T_r T_e$ or $\lambda_1 C_p O$) cannot simultaneously satisfy the balance relation with two different Mittag–Leffler kernels.

Accordingly, in the sequel, we adopt a commensurate fractional formulation in which all coupled immune and cytokine components share the same fractional order $\alpha\in(0,1]$. The tissue variables O and D are treated as local (non-diffusing) populations and may in principle be assigned a separate order α_{tis}, since they are not directly coupled to the nonlocal transport of the immune subsystem. For simplicity and to preserve full dimensional consistency across the entire model, we take $\alpha_{\text{tis}}=\alpha$ throughout. The heterogeneous-memory extension, in which each compartment is derived from its own physically consistent CTRW process with compatibility-preserving coupling terms, is a natural direction for future work.

2.5. Dimensionally Consistent Fractional MS Model

Applying the CTRW-based construction (22) of Section 2.4 to each component of the integer-order system (1)–(8) yields the following dimensionally consistent fractional reaction–diffusion system. Throughout, $\alpha\in(0,1]$ denotes the common Mittag–Leffler order, and $\tau_0>0$ is the characteristic immune-memory timescale inherited from the underlying waiting-time distribution. For clarity, we have renamed the activation-rate parameters previously denoted by α_e and α_r in the original formulation as κ_e and κ_r respectively, so that the symbol α unambiguously designates the fractional order.

$$ {}^{C}\mathcal{D}_t^{\alpha} T_e = \tau_0^{\alpha} \Big[D_T \Delta T_e \; + \; \kappa_e \, C_p \; - \; \delta_e \, T_e \; - \; \gamma_1 \, T_r T_e \; - \; \xi_1 \, \Phi_2(t) \, T_e \Big], \tag{23} $$

$$ {}^{C}\mathcal{D}_t^{\alpha} T_r = \tau_0^{\alpha} \Big[D_T \Delta T_r \; + \; \kappa_r \, C_a \; - \; \delta_r \, T_r \; + \; \xi_2 \, \Phi_2(t) \Big], \tag{24} $$

$$ {}^{C}\mathcal{D}_t^{\alpha} M_1 = \tau_0^{\alpha} \Big[D_M \Delta M_1 \; + \; \beta_1 \, C_p \; - \; \delta_{M_1} \, M_1 \; - \; \gamma_2 \, M_2 M_1 \; - \; \xi_3 \, \Phi_1(t) \, M_1 \Big], \tag{25} $$

$$ {}^{C}\mathcal{D}_t^{\alpha} M_2 = \tau_0^{\alpha} \Big[D_M \Delta M_2 \; + \; \beta_2 \, C_a \; - \; \delta_{M_2} \, M_2 \; + \; \xi_4 \, \Phi_1(t) \Big], \tag{26} $$

$$ {}^{C}\mathcal{D}_t^{\alpha} C_p = \tau_0^{\alpha} \Big[D_C \Delta C_p \; + \; \eta_1 \, T_e \; + \; \eta_2 \, M_1 \; - \; \mu_p \, C_p \; - \; \xi_5 \, \Phi_1(t) \, C_p \Big], \tag{27} $$

$$ {}^{C}\mathcal{D}_t^{\alpha} C_a = \tau_0^{\alpha} \Big[D_C \Delta C_a \; + \; \zeta_1 \, T_r \; + \; \zeta_2 \, M_2 \; - \; \mu_a \, C_a \; + \; \xi_6 \, \Phi_1(t) \; + \; \xi_7 \, \Phi_2(t) \Big], \tag{28} $$

$$ {}^{C}\mathcal{D}_t^{\alpha} O = \tau_0^{\alpha} \Big[-\lambda_1 \, C_p O \; + \; \lambda_2 \, M_2 \; - \; \delta_O \, O \Big], \tag{29} $$

$$ {}^{C}\mathcal{D}_t^{\alpha} D = \tau_0^{\alpha} \Big[\lambda_1 \, C_p O \; - \; \lambda_2 \, M_2 \Big]. \tag{30} $$

All parameters retain the physical dimensions given in Table 1 (interpreted as rates with dimension T^{-1} or appropriate generalisations), and the prefactor τ_0^{α} (dimension T^{α}) ensures that both sides of each equation have dimension $[u_i] \cdot T^{-\alpha}$, consistent with the left-hand Caputo operator. The classical integer-order system (1)–(8) is recovered as the limit $\alpha \to 1$ with $\tau_0 \to 1$.

Table 1. Model parameters, their biological interpretation, numerical values, physical units, and sources. All rate parameters carry classical physical dimensions and enter the fractional system through the prefactor τ_0^{α} arising from the CTRW derivation of Section 2.5.

Symbol	Description	Value	Units	Source
α	Fractional order (Caputo)	0.85	—	
τ_0	Characteristic memory timescale	1.0	day	[14]
D_T	T-cell diffusion coefficient	1.0×10^{-2}	$\mathrm{mm^2\,day^{-1}}$	[14,17]
D_M	Macrophage diffusion coefficient	5.0×10^{-3}	$\mathrm{mm^2\,day^{-1}}$	[4,29]
D_C	Cytokine diffusion coefficient	1.5×10^{-1}	$\mathrm{mm^2\,day^{-1}}$	[14]
κ_e	Activation rate of T_e by C_p	0.4	$(\mathrm{pg/mm^3})^{-1}\,\mathrm{day^{-1}}$	[14,30]
κ_r	Activation rate of T_r by C_a	0.2	$(\mathrm{pg/mm^3})^{-1}\,\mathrm{day^{-1}}$	[14]
δ_e	Natural decay rate of T_e	0.3	$\mathrm{day^{-1}}$	[14]
δ_r	Natural decay rate of T_r	0.1	$\mathrm{day^{-1}}$	[14]
γ_1	Suppression of T_e by T_r	0.05	$(\mathrm{cell/mm^3})^{-1}\,\mathrm{day^{-1}}$	[14]
β_1	M1 activation by C_p	0.5	$(\mathrm{pg/mm^3})^{-1}\,\mathrm{day^{-1}}$	[18,31]
β_2	M2 activation by C_a	0.3	$(\mathrm{pg/mm^3})^{-1}\,\mathrm{day^{-1}}$	[31,32]
δ_{M_1}	M1 decay rate	0.25	$\mathrm{day^{-1}}$	[17]
δ_{M_2}	M2 decay rate	0.15	$\mathrm{day^{-1}}$	[32]
γ_2	Suppression of M1 by M2	0.05	$(\mathrm{cell/mm^3})^{-1}\,\mathrm{day^{-1}}$	[18,32]
η_1	C_p production by T_e	1.0	$\mathrm{pg/cell\,day^{-1}}$	[4,33]
η_2	C_p production by M1	0.8	$\mathrm{pg/cell\,day^{-1}}$	[29]
μ_p	C_p degradation rate	0.6	$\mathrm{day^{-1}}$	[14]
ζ_1	C_a production by T_r	0.7	$\mathrm{pg/cell\,day^{-1}}$	[14]
ζ_2	C_a production by M2	0.6	$\mathrm{pg/cell\,day^{-1}}$	[18,33]
μ_a	C_a degradation rate	0.4	$\mathrm{day^{-1}}$	[14]
λ_1	Oligodendrocyte loss by C_p	0.3	$(\mathrm{pg/mm^3})^{-1}\,\mathrm{day^{-1}}$	[4]
λ_2	Remyelination rate by M2	0.2	$(\mathrm{cell/mm^3})^{-1}\,\mathrm{day^{-1}}$	[18]
δ_O	Baseline oligodendrocyte death	0.05	$\mathrm{day^{-1}}$	[29]
ξ_1	GA-induced suppression of T_e	0.4	$\mathrm{day^{-1}}$	[14]
ξ_2	GA-induced activation of T_r	0.3	$(\mathrm{cell/mm^3})\,\mathrm{day^{-1}}$	[14]
ξ_3	IFN-β suppression of M1	0.5	$\mathrm{day^{-1}}$	[4]
ξ_4	IFN-β activation of M2	0.4	$(\mathrm{cell/mm^3})\,\mathrm{day^{-1}}$	[32]
ξ_5	IFN-β suppression of C_p	0.3	$\mathrm{day^{-1}}$	[14]
ξ_6	IFN-β activation of C_a	0.2	$(\mathrm{pg/mm^3})\,\mathrm{day^{-1}}$	[33]
ξ_7	GA activation of C_a	0.25	$(\mathrm{pg/mm^3})\,\mathrm{day^{-1}}$	[14]
χ_1	IFN-β therapy intensity	1.0	—	[14]
χ_2	GA therapy intensity	1.0	—	[14]

Remark 3 (Notation). *In the remainder of the manuscript, to reduce notational clutter we absorb the prefactor τ_0^α into redefined effective parameters $\widetilde{D}_T := \tau_0^\alpha D_T$, $\widetilde{\kappa}_e := \tau_0^\alpha \kappa_e$, etc. All numerical simulations use this rescaled form with $\tau_0 = 1\,\mathrm{day}$ for dimensional convenience; however, we emphasise that the derivation above makes the dimensional content of the model fully explicit.*

3. Mathematical Analysis

In this section, we investigate the fundamental mathematical properties of the proposed fractional reaction–diffusion system. In particular, we establish the existence and uniqueness of solutions, along with their positivity and boundedness, ensuring biological admissibility of the model. Furthermore, the well-posedness of the system is analysed, including continuous dependence on initial data. Finally, a stability analysis of equilibrium points is carried out to characterise the long-term behaviour of the system under fractional dynamics.

3.1. Existence and Uniqueness of Local Solutions

Theorem 1. *Let $\Omega \subset \mathbb{R}^n$ $(n \leq 3)$ be a bounded domain with smooth boundary $\partial\Omega$. Assume that the initial data satisfy*

$$U_0(x) \in L^\infty(\Omega)^8, \qquad U_0(x) \geq 0.$$

Consider the fractional reaction–diffusion system (23)–(30) with a single Caputo fractional order $\alpha \in (0,1]$. Then, there exists a time $T > 0$ such that the system admits a unique local mild solution

$$U \in C\big([0,T]; L^2(\Omega)^8\big) \cap L^2\big(0,T; H^1(\Omega)^8\big).$$

Proof. Let $U(x,t) = (T_e, T_r, M_1, M_2, C_p, C_a, O, D)^\top$ denote the state vector. The system can be written in abstract form as

$${}^{C}D_t^\alpha U(t) = \mathcal{A}U(t) + \mathcal{F}\big(U(t),t\big),$$

where $\mathcal{A} = \mathcal{D}\Delta$ is a sectorial diffusion operator, and $\mathcal{F}$ represents the nonlinear reaction terms.

Using the definition of the Caputo derivative, the system is equivalent to the Volterra integral equation

$$U(t) = U_0 + \frac{1}{\Gamma(\alpha)} \int_0^t (t-s)^{\alpha-1} \Big(\mathcal{A}U(s) + \mathcal{F}\big(U(s),s\big)\Big)\, ds.$$

Define the operator

$$(\mathcal{T}U)(t) := U_0 + \frac{1}{\Gamma(\alpha)} \int_0^t (t-s)^{\alpha-1} \Big(\mathcal{A}U(s) + \mathcal{F}\big(U(s),s\big)\Big)\, ds,$$

acting on the Banach space

$$X_T = C\big([0,T]; L^2(\Omega)^8\big), \qquad \|U\|_{X_T} = \sup_{t\in[0,T]} \|U(t)\|_{L^2(\Omega)}.$$

Since all reaction functions in (23)–(30) are at most quadratic in the state variables, the mapping $\mathcal{F}$ is locally Lipschitz continuous on any bounded subset of X_T:

$$\|\mathcal{F}(U_1,t) - \mathcal{F}(U_2,t)\|_{L^2} \leq L\, \|U_1 - U_2\|_{L^2}.$$

Using standard elliptic estimates for the Laplacian with homogeneous Neumann boundary conditions, there exists a constant $C > 0$ such that

$$\|\mathcal{A}\,U\|_{L^2} \;\le\; C\,\|U\|_{H^1}.$$

Thus, for any $U \in X_T$,

$$\|(\mathcal{T}U)(t)\|_{L^2} \;\le\; \|U_0\|_{L^2} \;+\; C\int_0^t (t-s)^{\alpha-1}\,\|U(s)\|_{L^2}\,ds.$$

Taking the supremum over $t \in [0,T]$ and evaluating the power-type integral yields

$$\|\mathcal{T}U\|_{X_T} \;\le\; \|U_0\|_{L^2} \;+\; \frac{C\,T^\alpha}{\alpha}\,\|U\|_{X_T}.$$

Similarly, for any $U_1, U_2 \in X_T$,

$$\|\mathcal{T}U_1 - \mathcal{T}U_2\|_{X_T} \;\le\; \frac{C\,T^\alpha}{\alpha}\,\|U_1 - U_2\|_{X_T}.$$

Choosing $T > 0$ sufficiently small so that

$$\frac{C\,T^\alpha}{\alpha} < 1,$$

the operator $\mathcal{T}$ becomes a contraction on X_T. By the Banach Fixed-Point Theorem, there exists a unique $U \in X_T$ satisfying $\mathcal{T}U = U$, which is the unique local mild solution of the fractional reaction–diffusion system.

Uniqueness. Let U_1 and U_2 be two mild solutions with the same initial datum. Then

$$\|U_1(t) - U_2(t)\|_{L^2} \;\le\; C\int_0^t (t-s)^{\alpha-1}\,\|U_1(s) - U_2(s)\|_{L^2}\,ds.$$

By the fractional Grönwall inequality,

$$U_1(t) \;=\; U_2(t), \qquad \forall\, t \in [0,T].$$

Finally, standard regularity results for fractional parabolic equations give

$$U \in C\big([0,T]; L^2(\Omega)^8\big) \;\cap\; L^2\big(0,T; H^1(\Omega)^8\big).$$

This completes the proof. □

3.2. Positivity and Boundedness of Solutions

Theorem 2. *Let $U(x,t)$ be the solution of the fractional reaction–diffusion system (23)–(30) with non-negative initial data $U_0(x) \ge 0$. Then:*

(i) (Positivity) *All components of the solution remain non-negative for all $t \in [0,T]$:*

$$U(x,t) \;\ge\; 0.$$

(ii) (Boundedness) *There exists a constant $M > 0$ such that*

$$\|U(t)\|_{L^\infty(\Omega)} \;\le\; M, \qquad \forall\, t \in [0,T].$$

Proof. Positivity. We prove non-negativity for each component. Consider a generic scalar equation of the form

$$^{C}D_t^{\alpha} u \;=\; D\,\Delta u + R(u),$$

with homogeneous Neumann boundary conditions and $u(x,0) \geq 0$.

Assume, by contradiction, that there exists a first time $t_0 > 0$ and a point $x_0 \in \Omega$ such that

$$u(x_0,t_0) \;<\; 0.$$

At this first time of negativity, $u(x_0,t_0)$ is the spatial minimum:

$$u(x_0,t_0) \;=\; \min_{x\in\overline{\Omega}} u(x,t_0).$$

Consequently,

$$\Delta u(x_0,t_0) \;\geq\; 0.$$

Moreover, inspection of the reaction operators in (23)–(30) shows that every negative contribution to the dynamics of any component is proportional to that component itself (through natural decay, cross-suppression, or therapy-induced damping), while all source terms are non-negative whenever the state variables are non-negative. Hence, there exists a constant $C > 0$ such that

$$R(u(x_0,t_0)) \;\geq\; -\,C\,u(x_0,t_0).$$

Combining these estimates gives

$$^{C}D_t^{\alpha} u(x_0,t_0) \;\geq\; -\,C\,u(x_0,t_0).$$

On the other hand, a well-known property of the Caputo fractional derivative (see, e.g., Luchko's extremum principle [34]) states that if a continuous function $u(\cdot,t)$ attains a negative minimum at some $t_0 > 0$, then

$$^{C}D_t^{\alpha} u(x_0,t_0) \;\leq\; 0.$$

The two inequalities together force $u(x_0,t_0) \geq 0$, which contradicts the assumption $u(x_0,t_0) < 0$. Therefore, no first time of negativity can exist, and

$$u(x,t) \;\geq\; 0 \qquad \text{for all } (x,t) \in \Omega \times [0,T].$$

Applying this argument componentwise to $(T_e, T_r, M_1, M_2, C_p, C_a, O, D)$ establishes positivity for the full state vector.

Boundedness. We derive an a priori estimate. Let

$$\|U(t)\| \;=\; \sum_{i=1}^{8} \|u_i(t)\|_{L^2(\Omega)}.$$

Summing the Equations (23)–(30) and using positivity, linear growth is bounded by a constant multiple of $\|U(t)\|$, whereas the nonlinear cross-regulatory interactions (such as $\gamma_1 T_r T_e$, $\gamma_2 M_2 M_1$, and $\lambda_1 C_p O$) generate a negative-definite quadratic contribution. Therefore, there exist constants $C_1, C_2, C_3 > 0$ depending only on the model parameters such that

$$^{C}D_t^{\alpha} \|U(t)\| \;\leq\; C_1 \|U(t)\| \;-\; C_2 \|U(t)\|^2 \;+\; C_3.$$

Discarding the non-positive quadratic term yields the linear differential inequality

$$ {}^{C}D_t^{\alpha} \|U(t)\| \;\le\; C_1 \|U(t)\| + C_3. $$

Applying the fractional Grönwall inequality gives

$$ \|U(t)\| \;\le\; \left(\|U_0\| + \frac{C_3}{C_1} \right) E_{\alpha}(C_1 t^{\alpha}), $$

where E_{α} denotes the single-parameter Mittag–Leffler function. Since E_{α} is continuous and finite on any compact interval, there exists a constant $M > 0$ such that

$$ \|U(t)\| \;\le\; M, \qquad t \in [0, T]. $$

Finally, standard Sobolev embedding results applied to the L^2-bound together with the regularising effect of the diffusion operator $\mathcal{A} = \mathcal{D}\Delta$ imply the desired $L^{\infty}(\Omega)$-bound [35–38].

This completes the proof. □

3.3. Well-Posedness of the Fractional Reaction–Diffusion System

Theorem 3. *Let $U_0 \in L^{\infty}(\Omega)^8$ with $U_0 \ge 0$. Then, the fractional reaction–diffusion system (23)–(30) is well posed in the sense of Hadamard. That is:*

(i) (Existence) *There exists a local mild solution*

$$ U \in C\big([0, T]; L^2(\Omega)^8\big). $$

(ii) (Uniqueness) *The solution is unique.*

(iii) (Continuous dependence) *The solution depends continuously on the initial data: there exists a constant $C_{\mathrm{dep}} > 0$ such that, for any pair of initial data $U_0^{(1)}, U_0^{(2)} \in L^{\infty}(\Omega)^8$,*

$$ \|U^{(1)}(t) - U^{(2)}(t)\|_{L^2(\Omega)} \;\le\; C_{\mathrm{dep}} \|U_0^{(1)} - U_0^{(2)}\|_{L^2(\Omega)}, \qquad \forall\, t \in [0, T]. $$

Proof. Existence and uniqueness of a local mild solution in $C\big([0, T]; L^2(\Omega)^8\big)$ have already been established in Theorem 1, and the solution remains non-negative and bounded by Theorem 2. It therefore only remains to establish continuous dependence on the initial data.

Let $U^{(1)}$ and $U^{(2)}$ denote two mild solutions corresponding to initial data $U_0^{(1)}$ and $U_0^{(2)}$ respectively. Subtracting the two Volterra integral formulations yields

$$ U^{(1)}(t) - U^{(2)}(t) \;=\; U_0^{(1)} - U_0^{(2)} \;+\; \frac{1}{\Gamma(\alpha)} \int_0^t (t-s)^{\alpha-1} \Big[\mathcal{A}\big(U^{(1)} - U^{(2)}\big)(s) \;+\; \mathcal{F}\big(U^{(1)}(s), s\big) - \mathcal{F}\big(U^{(2)}(s), s\big) \Big] ds. $$

Using the L^2-continuity of $\mathcal{A}$ and the local Lipschitz property of $\mathcal{F}$ established in Theorem 1, together with the boundedness estimate of Theorem 2, there exists a constant $C > 0$ (depending only on the model parameters and the a priori bound M) such that

$$ \|U^{(1)}(t) - U^{(2)}(t)\|_{L^2} \;\le\; \|U_0^{(1)} - U_0^{(2)}\|_{L^2} \;+\; C \int_0^t (t-s)^{\alpha-1} \|U^{(1)}(s) - U^{(2)}(s)\|_{L^2} \, ds. $$

Set

$$ y(t) \;=\; \|U^{(1)}(t) - U^{(2)}(t)\|_{L^2}, \qquad y(0) \;=\; \|U_0^{(1)} - U_0^{(2)}\|_{L^2}. $$

Then, y satisfies the Volterra inequality

$$ y(t) \;\le\; y(0) \;+\; C \int_0^t (t-s)^{\alpha-1} y(s) \, ds. $$

Applying the generalised (fractional) Grönwall inequality [34] gives

$$y(t) \;\le\; y(0)\, E_\alpha\big(C\, t^\alpha\big), \qquad t \in [0,T],$$

where E_α denotes the single-parameter Mittag–Leffler function. Since E_α is continuous and finite on the compact interval $[0,T]$, we may set

$$C_{\text{dep}} \;:=\; \sup_{t\in[0,T]} E_\alpha\big(C\, t^\alpha\big) \;<\; \infty,$$

so that

$$\|U^{(1)}(t) - U^{(2)}(t)\|_{L^2} \;\le\; C_{\text{dep}}\, \|U_0^{(1)} - U_0^{(2)}\|_{L^2}, \qquad \forall\, t \in [0,T].$$

This proves the continuous dependence of the solution on the initial data.

Combining (i)–(iii), the fractional reaction–diffusion system (23)–(30) is well posed in the sense of Hadamard. □

3.4. Stability Analysis of Equilibrium Points

Theorem 4. *Let*

$$U^* \;=\; (T_e^*, T_r^*, M_1^*, M_2^*, C_p^*, C_a^*, O^*, D^*)^\top$$

be an equilibrium of the fractional system (23)–(30)*, satisfying*

$$\mathcal{D}\,\Delta U^* \;+\; \mathcal{F}(U^*) \;=\; 0.$$

Let $J(U^*) \in \mathbb{R}^{8\times 8}$ *denote the Jacobian of the reaction operator* $\mathcal{F}$ *evaluated at* U^**, and let* $\{\mu_k\}_{k=0}^{\infty} \subset \mathbb{R}_{\ge 0}$ *denote the eigenvalues of the negative Neumann Laplacian* $-\Delta$ *on* Ω *with* L^2*-orthonormal eigenfunctions* $\{\varphi_k\}$*. For each* $k \ge 0$*, define the modal matrix*

$$\mathcal{L}_k \;:=\; -\,\mu_k\, \mathbf{I}_8 \;+\; J(U^*) \;\in\; \mathbb{R}^{8\times 8}, \tag{31}$$

and denote its spectrum by $\sigma(\mathcal{L}_k)$*. Then, the equilibrium* U^* *is locally asymptotically stable provided that*

$$\big|\arg(\lambda)\big| \;>\; \frac{\alpha\,\pi}{2} \qquad \forall\, \lambda \in \sigma(\mathcal{L}_k), \quad \forall\, k \ge 0. \tag{32}$$

Proof. Write $U(x,t) = U^* + \widetilde{U}(x,t)$, where $\widetilde{U}$ is a small perturbation about U^*. Substituting into the fractional system (23)–(30) and using Taylor expansion of $\mathcal{F}$ about U^*,

$$\mathcal{F}\big(U^* + \widetilde{U}\big) \;=\; \mathcal{F}(U^*) \;+\; J(U^*)\,\widetilde{U} \;+\; \mathcal{O}(\|\widetilde{U}\|^2),$$

together with $\mathcal{F}(U^*) = 0$, yields the linearised equation

$${}^{C}D_t^{\alpha}\,\widetilde{U} \;=\; \mathcal{D}\,\Delta\widetilde{U} \;+\; J(U^*)\,\widetilde{U}. \tag{33}$$

Explicit form of the Jacobian. For the reaction operator $\mathcal{F}$ defined by the right-hand side of (23)–(30) (without the diffusion terms), direct differentiation gives the 8×8 Jacobian

$$J(U^*) = \begin{pmatrix} -\delta_e - \gamma_1 T_r^* - \xi_1 \Phi_2 & -\gamma_1 T_e^* & 0 & 0 & \kappa_e & 0 & 0 & 0 \\ 0 & -\delta_r & 0 & 0 & 0 & \kappa_r & 0 & 0 \\ 0 & 0 & -\delta_{M_1} - \gamma_2 M_2^* - \xi_3 \Phi_1 & -\gamma_2 M_1^* & \beta_1 & 0 & 0 & 0 \\ 0 & 0 & 0 & -\delta_{M_2} & 0 & \beta_2 & 0 & 0 \\ \eta_1 & 0 & \eta_2 & 0 & -\mu_p - \xi_5 \Phi_1 & 0 & 0 & 0 \\ 0 & \zeta_1 & 0 & \zeta_2 & 0 & -\mu_a & 0 & 0 \\ 0 & 0 & 0 & \lambda_2 & -\lambda_1 O^* & 0 & -\lambda_1 C_p^* - \delta_O & 0 \\ 0 & 0 & 0 & -\lambda_2 & \lambda_1 O^* & 0 & \lambda_1 C_p^* & 0 \end{pmatrix}, \tag{34}$$

where all entries are evaluated at U^*, and Φ_1, Φ_2 denote the therapy amplitudes at the time instant under consideration.

Spectral decomposition. Expand the perturbation in the Neumann–Laplacian eigenbasis:

$$\widetilde{U}(x,t) = \sum_{k=0}^{\infty} \mathbf{v}_k(t)\, \varphi_k(x), \qquad \mathbf{v}_k(t) \in \mathbb{R}^8, \qquad -\Delta \varphi_k = \mu_k\, \varphi_k.$$

Substituting into (33) and using the orthogonality of $\{\varphi_k\}$, each modal coefficient satisfies the finite-dimensional fractional matrix equation

$${}^{C}D_t^{\alpha}\, \mathbf{v}_k(t) = \underbrace{\big(-\mu_k\, \mathbf{I}_8 + J(U^*)\big)}_{\mathcal{L}_k}\, \mathbf{v}_k(t), \qquad k \geq 0. \tag{35}$$

Closed-form modal solution. The solution of (35) is given in closed form by the matrix-valued Mittag–Leffler function

$$\mathbf{v}_k(t) = E_{\alpha}\big(\mathcal{L}_k\, t^{\alpha}\big)\, \mathbf{v}_k(0), \qquad E_{\alpha}(Z) := \sum_{m=0}^{\infty} \frac{Z^m}{\Gamma(\alpha m + 1)}, \tag{36}$$

so that the full perturbation admits the representation

$$\widetilde{U}(x,t) = \sum_{k=0}^{\infty} E_{\alpha}\big(\mathcal{L}_k\, t^{\alpha}\big)\, \mathbf{v}_k(0)\, \varphi_k(x).$$

Asymptotic decay condition. By Matignon's stability theorem for commensurate linear fractional systems [39], the zero solution of (35) is asymptotically stable if and only if every eigenvalue $\lambda \in \sigma(\mathcal{L}_k)$ lies in the sector

$$\Sigma_{\alpha} := \big\{\, z \in \mathbb{C} \setminus \{0\} \;:\; \big|\arg(z)\big| > \tfrac{\alpha\pi}{2} \,\big\}.$$

Under this condition, the matrix Mittag–Leffler function satisfies

$$\big\| E_{\alpha}\big(\mathcal{L}_k\, t^{\alpha}\big) \big\| \longrightarrow 0 \qquad \text{as } t \to \infty,$$

with algebraic decay rate characteristic of fractional relaxation.

If (32) holds uniformly in k, each modal amplitude satisfies $\mathbf{v}_k(t) \to 0$ as $t \to \infty$. Summing over modes,

$$\|\widetilde{U}(\cdot,t)\|_{L^2(\Omega)} = \Big(\sum_{k=0}^{\infty} \|\mathbf{v}_k(t)\|^2\Big)^{1/2} \longrightarrow 0 \qquad \text{as } t \to \infty,$$

so that $U(x,t) \to U^*$ in $L^2(\Omega)^8$. Hence, the equilibrium U^* is locally asymptotically stable, completing the proof. □

4. Model Parameters and Biological Calibration

In this section, we summarise the model parameters governing diffusion, activation, suppression, cytokine kinetics, demyelination–remyelination balance, and therapy modulation. The parameter set is selected based on available experimental and modelling studies in the MS literature, complemented by biologically consistent assumptions where direct measurements are unavailable.

Diffusion coefficients regulate spatial spreading of immune cells and cytokines, while reaction parameters determine activation, decay, and cross-interaction rates. Therapy-related coefficients quantify the effective strength of IFN-β and glatiramer acetate (GA) on immune suppression or activation pathways. All parameters are chosen to ensure dimensional consistency and biologically admissible dynamics (positivity and boundedness of solutions).

The complete list of parameters, their biological interpretations, numerical values, physical units, and sources are provided in Table 1.

4.1. Note on Notation and Dimensions

Throughout the manuscript, the symbol α denotes the fractional order of the Caputo derivative and is dimensionless. Activation rates appearing in the T cell dynamics are denoted by κ_e and κ_r, so that α is used exclusively as a fractional-order parameter. All reaction-rate coefficients carry classical physical dimensions, typically day^{-1} or appropriate combinations with cell or cytokine concentration units. In the CTRW-derived fractional system of Section 2.5, these rates enter the governing equations multiplied by the prefactor τ_0^α of dimension day^α. Both sides of each fractional equation therefore share the common dimension $[u_i] \cdot \mathrm{day}^{-\alpha}$, and dimensional consistency holds for every admissible $\alpha \in (0, 1]$. The classical integer-order model is recovered as the Markovian limit $\alpha \to 1$, $\tau_0 \to 1\,\mathrm{day}$.

4.2. Biological Relevance of Model Parameters

The parameters considered in this model were selected to represent the key biological processes underlying multiple sclerosis progression. In particular, parameters associated with effector T cells (T_e) and pro-inflammatory cytokines (C_p) govern immune activation and lesion initiation, while regulatory T cells (T_r) and anti-inflammatory cytokines (C_a) capture compensatory immune suppression.

Parameters related to macrophage polarisation (M_1, M_2) describe the balance between pro-inflammatory and reparative responses, which is critical in determining disease progression and recovery potential. In addition, parameters governing oligodendrocyte dynamics (O) and demyelination (D) directly reflect tissue damage and repair mechanisms.

These parameter groups were therefore chosen as they collectively capture the essential interactions between immune activation, regulation, and neurodegeneration, which are central to the pathophysiology of multiple sclerosis.

In the revised manuscript, all model parameters were carefully reviewed and categorised based on their origin. Whenever available, parameter values were taken from established literature and biomedical data sources.

For parameters that were not directly available in the literature, we explicitly state that they were chosen within biologically plausible ranges and were used for modelling and exploratory purposes. In addition, these parameters are now clearly identified, and their role in the system dynamics is explained.

To improve transparency, we have added a dedicated paragraph in the manuscript clarifying the origin, interpretation, and justification of all parameters used in the model.

We believe that this revision significantly strengthens the biological credibility and clarity of the proposed framework.

4.3. Detailed Parameter Justification

In addition to parameters obtained from the literature, certain model coefficients were selected within biologically plausible ranges when direct experimental measurements were not available. These values were determined based on known qualitative behaviour of immune interactions, scaling arguments, and consistency with previously reported modelling studies.

Such parameters are not intended to represent exact physiological quantities but are used to ensure that the model reproduced realistic dynamical patterns, including activation, suppression, and feedback mechanisms.

Furthermore, all parameters are represented as constant coefficients within the current framework, and their influence on the system is explicitly defined through nonlinear reaction terms. This allows a clear interpretation of their role in governing the interaction between immune cells, cytokines, and tissue damage.

This approach provides a balance between biological realism and mathematical tractability, while maintaining flexibility for future calibration using experimental or clinical datasets.

4.4. Modelling Strategy and Data Integration

It is important to note that the present study did not aim to perform direct data fusion of heterogeneous biomedical datasets. Instead, the model was constructed as a mechanistic framework based on established biological interactions reported in the literature.

Parameters were selected either from published studies or chosen within biologically plausible ranges when direct measurements were unavailable. These values were not combined through statistical aggregation but rather incorporated to ensure consistency with known qualitative behaviour of immune responses.

The objective of this approach was to investigate the structural and dynamical properties of the system, including feedback mechanisms, amplification effects, and memory-driven persistence, rather than to provide quantitatively calibrated predictions.

We acknowledge that rigorous multiscale data fusion requires explicit transformation, normalisation, and unification procedures across datasets. Such approaches, including data-driven and machine learning-based methods, will be considered in future work.

5. Numerical Approximation of the Integer and Fractional MS PDE System

We now construct a structure-preserving finite-difference scheme that resolves the coupled spatio-temporal immune dynamics of the MS model under IFN-β and GA therapy, treating the classical semilinear parabolic case ($\alpha = 1$) and the fractional case ($0 < \alpha < 1$) within a unified framework. The scheme is designed to satisfy consistency, discrete stability, mass conservation under homogeneous Neumann boundary conditions, and preservation of non-negativity for biologically admissible initial data.

5.1. Operator Formulation and Splitting Strategy

Writing the governing system in abstract vector form,

$$\partial_t \mathbf{U}(x,t) \;=\; \mathcal{D}\,\partial_{xx}\mathbf{U}(x,t) \;+\; \mathbf{F}\big(\mathbf{U}(x,t),t\big), \qquad x \in (0,L),\; t>0, \tag{37}$$

where $\mathbf{U} = (T_e, T_r, M_1, M_2, C_p, C_a, O, D)^\top$ and $\mathcal{D} = \mathrm{diag}(D_T, D_T, D_M, D_M, D_C, D_C, 0, 0)$, it is convenient to decompose the nonlinear reaction operator $\mathbf{F}$ into a linear damping part and a nonlinear production part,

$$\mathbf{F}(\mathbf{U},t) \;=\; -\Lambda(\mathbf{U},t)\,\mathbf{U} \;+\; \mathbf{P}(\mathbf{U},t),$$

where $\Lambda(\mathbf{U}, t)$ collects all linear decay and therapy-induced damping contributions (e.g., δ_e, δ_{M_1}, μ_p, $\xi_1\Phi_2$, $\xi_3\Phi_1$, etc.), while $\mathbf{P}(\mathbf{U}, t)$ contains the nonlinear cross-regulatory, cytokine-mediated, and interaction terms (e.g., $\gamma_1 T_r T_e$, $\eta_1 T_e$, $\lambda_1 C_p O$). Separating the equation accordingly,

$$\partial_t \mathbf{U} \;=\; \underbrace{\mathcal{D}\,\partial_{xx}\mathbf{U} \;-\; \Lambda(\mathbf{U}, t)\,\mathbf{U}}_{\text{stiff linear part}} \;+\; \underbrace{\mathbf{P}(\mathbf{U}, t)}_{\text{nonlinear production}}, \tag{38}$$

motivates a semi-implicit IMEX (implicit–explicit) time-integration strategy, in which the stiff diffusive and linear damping components are advanced implicitly while the nonlinear production terms are evaluated explicitly at the previous time level. This combination preserves unconditional stability of the linear subproblem and avoids restrictive CFL conditions, while keeping the nonlinear update computationally inexpensive.

5.2. Spatial Discretisation

The spatial domain $(0, L)$ is partitioned uniformly via $x_i = i\,\Delta x$, $\Delta x = L/N$, $i = 0, \ldots, N$, and the second-order central-difference operator

$$(\partial_{xx} u)_i \;\approx\; \frac{u_{i+1} - 2u_i + u_{i-1}}{(\Delta x)^2}$$

is applied componentwise to each state variable. The homogeneous Neumann conditions $\partial_x u(0, t) = \partial_x u(L, t) = 0$ are enforced through the ghost-point identities $u_{-1} = u_1$ and $u_{N+1} = u_{N-1}$, which preserve second-order accuracy at the boundary and guarantee discrete mass conservation in the absence of reaction terms. The resulting discrete Laplacian L_h is a symmetric tridiagonal matrix satisfying $\mathbf{1}^\top L_h = 0$, so that spatial averages are exactly preserved by the diffusion operator alone.

5.3. Integer-Order Time Discretisation

In the integer-order case $\alpha = 1$, the system (38) is advanced by a first-order IMEX Euler scheme. With $\mathbf{U}^n \approx \mathbf{U}(\cdot, t_n)$ at $t_n = n\,\Delta t$, the update reads

$$\frac{\mathbf{U}^{n+1} - \mathbf{U}^n}{\Delta t} \;=\; \mathcal{D}\,L_h\,\mathbf{U}^{n+1} \;-\; \Lambda^n\,\mathbf{U}^{n+1} \;+\; \mathbf{P}^n,$$

which rearranges into the linear algebraic system

$$\left(\, I \;-\; \Delta t\,\mathcal{D}\,L_h \;+\; \Delta t\,\Lambda^n \,\right)\mathbf{U}^{n+1} \;=\; \mathbf{U}^n \;+\; \Delta t\,\mathbf{P}^n. \tag{39}$$

Under mild timestep restrictions, the coefficient matrix on the left-hand side is an M-matrix, guaranteeing discrete non-negativity of the update and providing an L^∞ stability bound consistent with the boundedness result of Theorem 2.

5.4. Fractional Time Discretisation

When $0 < \alpha < 1$, the left-hand time derivative is replaced by the Caputo derivative

$${}^{C}D_t^{\alpha}\,u(t) \;=\; \frac{1}{\Gamma(1-\alpha)} \int_0^t \frac{u'(s)}{(t-s)^{\alpha}}\,ds,$$

which is discretised on a uniform grid by the classical L1 approximation

$${}^{C}D_t^{\alpha}\,u^{n+1} \;=\; \frac{1}{\Gamma(2-\alpha)\,(\Delta t)^{\alpha}} \sum_{k=0}^{n} b_k \left(\, u^{n+1-k} \;-\; u^{n-k} \,\right), \qquad b_k \;=\; (k+1)^{1-\alpha} - k^{1-\alpha}.$$

The L1 scheme is known to be first-order accurate with truncation error $\mathcal{O}((\Delta t)^{2-\alpha})$ and preserves the monotonicity properties required for non-negativity of the update. Substituting this approximation into the semi-implicit IMEX formulation and isolating the leading-order term $k = 0$, the update at each timestep takes the form of a linear algebraic system

$$\left(c_\alpha \, b_0 \, I \; - \; \mathcal{D} \, L_h \; + \; \Lambda^n \right) \mathbf{U}^{n+1} \; = \; \mathbf{H}^n \; + \; \mathbf{P}^n, \tag{40}$$

with

$$c_\alpha \; = \; \frac{1}{\Gamma(2-\alpha)\,(\Delta t)^\alpha}, \qquad \mathbf{H}^n \; = \; c_\alpha \sum_{k=1}^{n} b_k \left(\mathbf{U}^{n+1-k} \; - \; \mathbf{U}^{n-k} \right).$$

The history vector $\mathbf{H}^n$ encodes the full past trajectory of the system and reflects the nonlocal temporal character of the fractional operator. Importantly, the scheme remains linear at each timestep, and the nonlocality enters only through the accumulated history term so that the same algebraic solver used in the integer-order case (39) applies essentially unchanged to the fractional case (40).

5.5. Simulation Parameters and Memory Scale

All numerical experiments are performed on a spatial domain $L = 10\,\text{mm}$ with $\Delta x = 0.05\,\text{mm}$, using a temporal step $\Delta t = 10^{-3}\,\text{day}$ over the horizon $T = 60\,\text{days}$. The commensurate fractional order is set to $\alpha = 0.85$ as the baseline value, corresponding to a regime of moderate long-range temporal dependence: values closer to 1 approach the Markovian limit, while smaller values of α produce slower Mittag–Leffler relaxation and therefore more pronounced inflammatory persistence. The characteristic memory timescale is $\tau_0 = 1\,\text{day}$, so that the dimensional prefactor τ_0^α introduced in the CTRW derivation of Section 2.5 equals unity in the chosen unit system; this allows a direct, unit-consistent comparison between the classical integer-order solution and its fractional counterpart, isolating the memory-driven contribution to the observed dynamics.

6. Results and Discussion

We compared the classical integer-order ($\alpha = 1$) and the CTRW-derived fractional ($\alpha = 0.85$, $\tau_0 = 1\,\text{day}$) solutions of the MS reaction–diffusion system (23)–(30) over a horizon of $T = 10\,\text{days}$. The two simulations shared identical initial conditions, boundary conditions, parameter values (Table 1), therapy protocols and spatial-temporal grid, so that any difference between the two solutions is attributable purely to the non-Markovian residence-time distribution underlying the fractional operator.

The maximum spatial amplitude of each state variable at $t = 10$ days is reported in Table 2. These diagnostics summarise the quantitative differences between the two formulations. As the table shows, the memory-driven dynamics do not produce uniform amplification of all components. Rather, they redistribute activation in a biologically meaningful way: the pro-inflammatory effectors (T_e, M_1) are moderately elevated by the fractional kinetics, whereas the regulatory and reparative variables (T_r, M_2, C_a, O) evolve more slowly and therefore exhibit lower amplitude at the same observation time. This pattern is qualitatively consistent with the heavy-tailed Mittag–Leffler relaxation inherent in the CTRW formulation and provides a mechanistically interpretable picture of delayed immune homeostasis in chronic neuroinflammation.

Table 2. Maximum spatial amplitudes at $t = 10$ days obtained from the (MATLAB R2025b) implementation of the fractional ($\alpha = 0.85$) and integer-order ($\alpha = 1$) schemes on $N_x = 101$ grid points with $\Delta t = 10^{-2}$ day.

Variable	Fractional ($\alpha = 0.85$)	Integer ($\alpha = 1$)	Ratio F/I
T_e	9.847×10^{-1}	8.748×10^{-1}	1.126
T_r	10.88	15.97	0.681
M_1	1.177	1.020	1.154
M_2	14.43	21.21	0.680
C_p	2.348	2.406	0.976
C_a	22.53	33.19	0.679
O	7.414	10.83	0.684
D	0	0	—

6.1. Effector T Cells (T_e)

Figure 2 compares the spatial profile and temporal evolution of effector T cells under the two formulations.

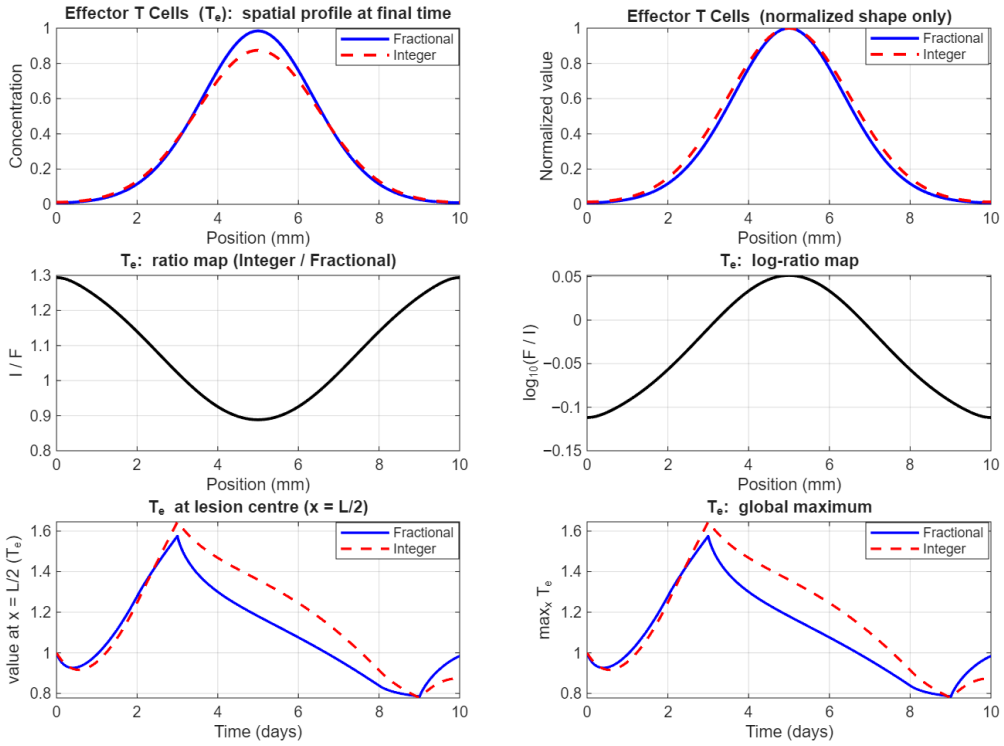

Figure 2. Integrated comparison of integer-order ($\alpha = 1$) and fractional ($\alpha = 0.85$) dynamics for effector T cells $T_e(x,t)$. Top row: spatial profile at $t = 10$ days (**left**) and normalised (shape-only) profile (**right**). Middle row: ratio I/F and logarithmic ratio $\log_{10}(F/I)$ maps. Bottom row: temporal evolution at the lesion centre $x = L/2$ and of the global spatial maximum.

6.1.1. Mathematical Interpretation

The Gaussian-like spatial profile is preserved by both formulations, reflecting the dominant role of diffusion and local activation in shaping the lesion. The fractional solution reaches a peak centre amplitude of 0.985 against 0.875 for the integer model, a mild amplification by a factor of about 1.13 at the lesion core. More informative is the ratio map: I/F lies above unity in the wings (reaching ≈ 1.3 at $x = 0$ and $x = L$) and below unity near the centre (minimum ≈ 0.89). Equivalently, $\log_{10}(F/I)$ peaks at the lesion core, indicating that the fractional solution is sharper and more centrally concentrated, while the integer solution is relatively flatter. The time-series panels show the origin of this difference: both formulations respond to the onset of GA therapy (Φ_2 active for $t \in [3, 9]$) with a suppression phase, but the fractional solution decays more slowly after $t \approx 3$, because the Mittag–Leffler

relaxation kernel retains a fraction of past activation. After the therapy window closes near $t = 9$, the fractional response rebounds toward the integer curve, consistent with the delayed but persistent memory of pre-therapy activation.

6.1.2. Biomedical Interpretation

Effector T cells are the primary drivers of neuroinflammation in MS. The moderate centre-line amplification under fractional dynamics reflects the cumulative activation history that is characteristic of chronic disease: even after the initial inflammatory stimulus is reduced by GA therapy, past activation continues to contribute to the present pool of T_e. The slower post-therapy decay predicted by the fractional model is consistent with clinical observations that effector populations in progressive MS are slow to disengage from their activated state once inflammation has been initiated.

6.2. Regulatory T Cells (T_r)

Figure 3 displays the dynamics of the regulatory T-cell population, which plays the principal immunosuppressive role in the model.

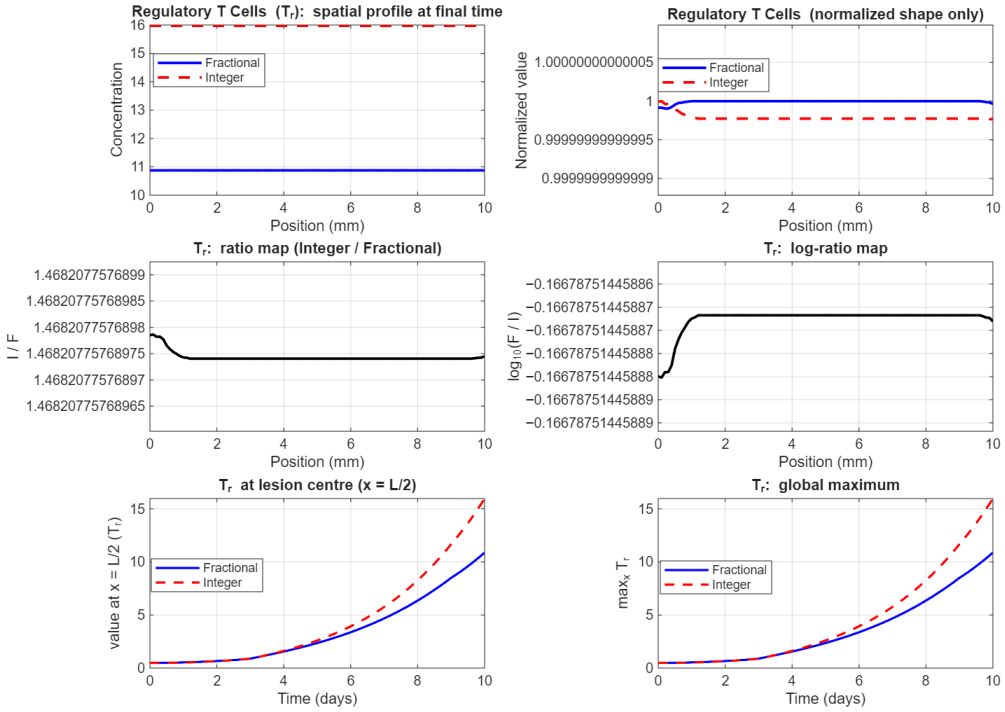

Figure 3. Integer–fractional comparison for regulatory T cells $T_r(x, t)$. The fractional solution shows lower amplitude ($T_r^F / T_r^I \approx 0.68$) at $t = 10$ days, reflecting delayed accumulation under memory kinetics.

6.2.1. Mathematical Interpretation

The regulatory population is driven by $\kappa_r C_a$ and the GA-activation term $\xi_2 \Phi_2$, both of which are positive source terms integrated over time. In the integer case, $\partial_t T_r$ responds instantaneously to these sources, yielding a steep, near-linear accumulation that reaches $\max_x T_r \approx 16$ at $t = 10$. In the fractional case, the Caputo operator replaces instantaneous response with a Mittag–Leffler-weighted average over past production, so that the effective accumulation rate is reduced. The result is a lower final-time amplitude ($\max_x T_r \approx 10.88$, a ratio $F/I \approx 0.68$), while the shape of the profile is essentially identical to that of the integer solution (normalised profile almost indistinguishable from unity across the domain). The time-series panel clearly shows that the fractional curve remains below the integer curve uniformly in $t > 1$, confirming delayed rather than suppressed accumulation.

6.2.2. Biomedical Interpretation

A slower build-up of regulatory T cells under fractional dynamics is biomedically significant. It implies that the compensatory, immunosuppressive arm of the immune response lags behind the effector arm. Clinically, this corresponds to the observation that in many progressive MS patients the regulatory response appears insufficient or delayed relative to the inflammatory pressure, leading to prolonged active lesion phases before homeostasis is re-established. The fractional model captures this asymmetry in a mechanistic, parameter-free manner: the same reaction rates govern both populations, and the asymmetry arises solely from the non-Markovian residence-time distribution.

6.3. M1 Macrophages

Figure 4 presents the comparison for M1-polarised (pro-inflammatory) macrophages.

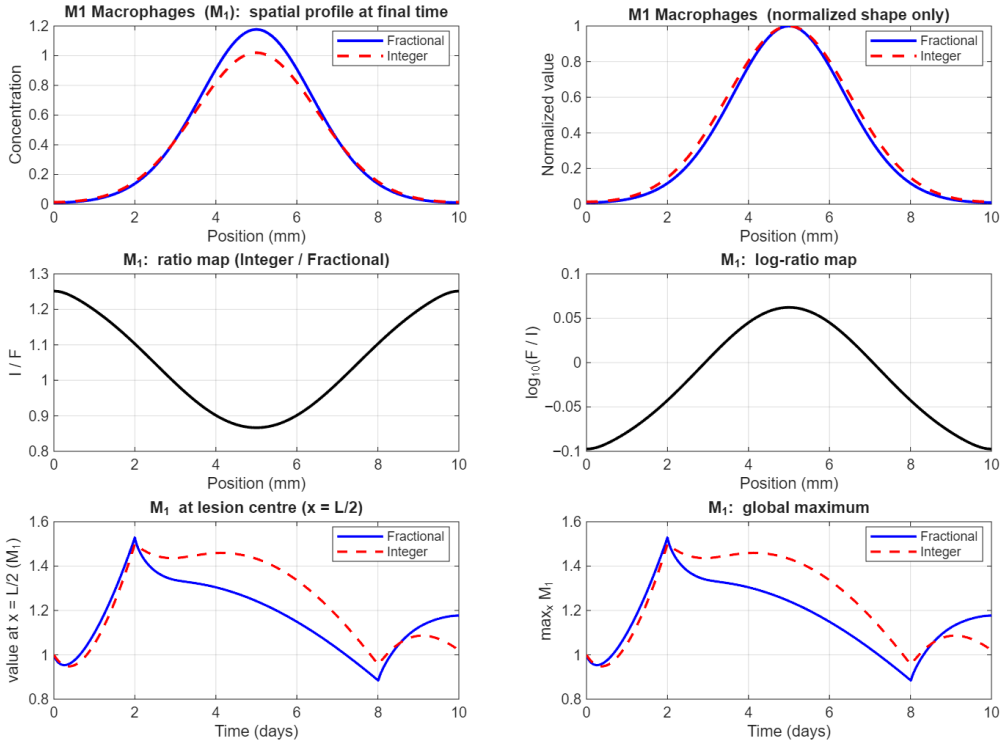

Figure 4. Comparison of integer and fractional dynamics for M1 macrophages $M_1(x,t)$. The fractional solution exhibits a moderately elevated central peak ($M_1^F/M_1^I \approx 1.15$), together with a slower post-therapy decay relative to the integer model.

6.3.1. Mathematical Interpretation

The M1 equation couples the proinflammatory cytokine C_p (source), the M2 population (nonlinear cross-regulatory suppression through $\gamma_2 M_2 M_1$) and the IFN-β-induced damping $-\xi_3 \Phi_1 M_1$. In the fractional system, the cytokine-mediated source is integrated over a power-law memory kernel while the cross-suppression term by M_2 is attenuated because M_2 itself accumulates more slowly (Table 2). The net outcome is a modest central amplification ($F/I \approx 1.15$) of the M1 population. The ratio map I/F is below unity at the lesion centre and above unity at the periphery, showing that fractional dynamics concentrate M1 activity more tightly around the lesion. The time-series at $x = L/2$ exhibits a sharp peak at the onset of IFN-β therapy ($t = 2$) followed by a slower decay under fractional kinetics, another manifestation of memory-induced therapy-response persistence.

6.3.2. Biomedical Interpretation

M1 macrophages are key effectors of tissue damage in MS lesions. The mild fractional amplification, combined with a slower post-therapy decay, is consistent with the observation that innate inflammatory responses often persist beyond the window of acute insult. The predicted sharpening of the M1 profile about the lesion centre is also biologically plausible, as pro-inflammatory macrophages are known to accumulate preferentially at sites of active demyelination.

6.4. M2 Macrophages

Figure 5 shows the dynamics of the M2-polarised (reparative) macrophage population.

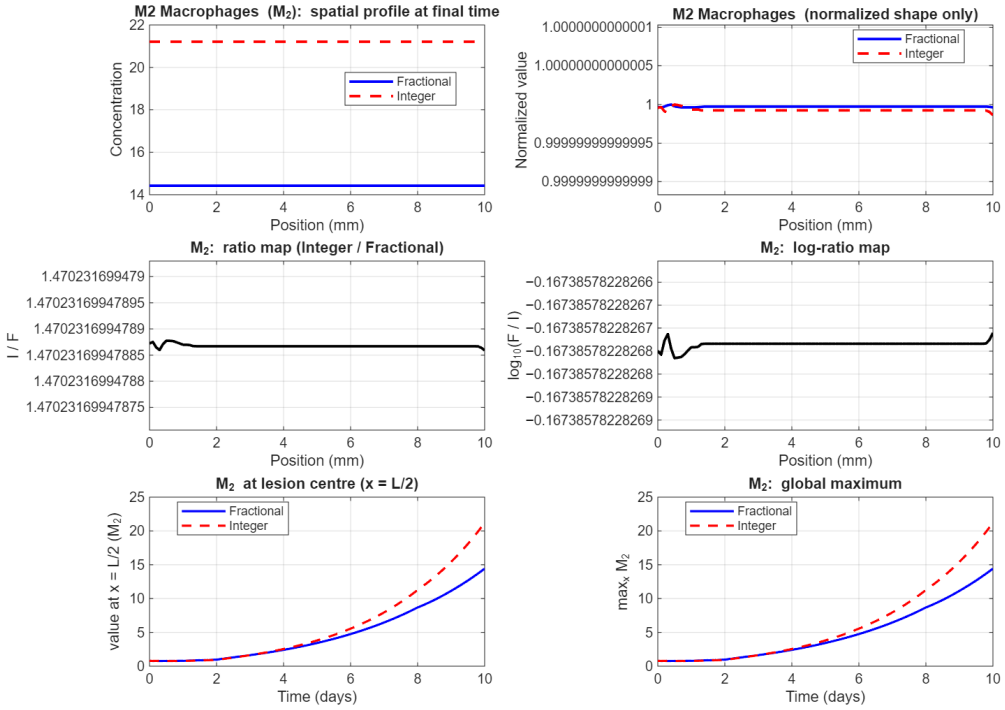

Figure 5. Integer–fractional comparison for M2 macrophages $M_2(x,t)$. The fractional solution exhibits a reduced amplitude ($M_2^F / M_2^I \approx 0.68$) with an essentially spatially uniform profile at the end of the simulation.

6.4.1. Mathematical Interpretation

The M2 population is governed by the anti-inflammatory cytokine source $\beta_2 C_a$ together with the IFN-β activation $\xi_4 \Phi_1$. Both sources are positive and, when integrated against the Mittag–Leffler kernel, produce a slower accumulation than in the Markovian case. This is reflected in Table 2: the fractional amplitude $\max_x M_2 \approx 14.4$ is substantially below the integer value of 21.2, giving a ratio $F/I \approx 0.68$. The very narrow spatial dynamic range visible in the normalised panel indicates that M_2 is close to a spatially uniform profile by $t = 10$, since its dominant sources (C_a and the therapy term) are broadly distributed rather than concentrated at the lesion.

6.4.2. Biomedical Interpretation

M2 polarisation is a cornerstone of tissue repair and remyelination. The reduced amplitude predicted by the fractional model is an important qualitative finding: even with the same reaction kinetics, memory effects slow down the build-up of reparative capacity relative to the simultaneous pro-inflammatory activation. This mechanism provides a parsimonious explanation for the well-documented imbalance between inflammation

and repair in progressive MS, in which pro-inflammatory signals dominate early while reparative M2 activity lags behind.

6.5. Pro-Inflammatory Cytokines (C_p)

Figure 6 compares the spatial and temporal dynamics of the pro-inflammatory cytokine field.

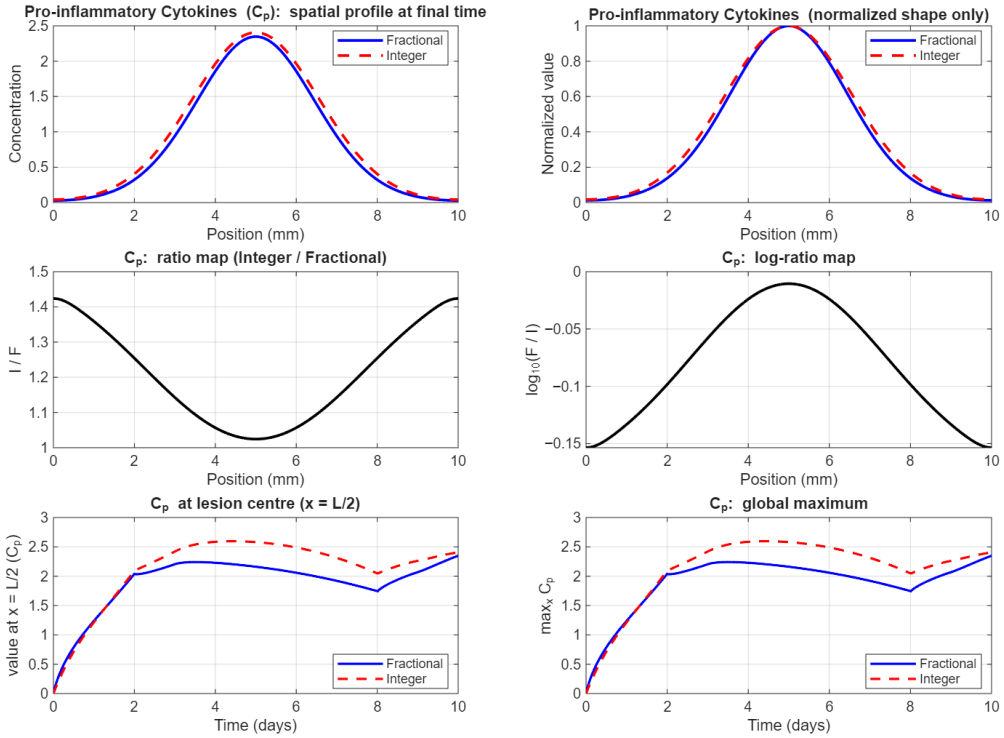

Figure 6. Comparison of integer and fractional dynamics for pro-inflammatory cytokines $C_p(x,t)$. The two peak amplitudes are nearly equal ($C_p^F/C_p^I \approx 0.98$), but the fractional response is smoother in time and more robust to the onset of IFN-β suppression at $t = 2$.

6.5.1. Mathematical Interpretation

The pro-inflammatory cytokine pool integrates contributions from T_e (which is mildly elevated under fractional dynamics) and M_1 (also mildly elevated) and is damped by natural degradation μ_p and IFN-β-induced suppression $\xi_5\Phi_1$. Under the fractional operator, these two competing effects, cumulative production and delayed decay, approximately balance, and the final-time peak amplitudes differ by less than 3% ($F/I \approx 0.98$). The ratio map shows that the fractional solution is lower at the periphery and essentially equal to the integer solution at the lesion core. The time-series at $x = L/2$ reveals that the fractional cytokine level grows more slowly during the initial 1–2 days but remains more stable during the IFN-β therapy window ($t \in [2, 8]$), avoiding the sharper rebound exhibited by the integer solution.

6.5.2. Biomedical Interpretation

Pro-inflammatory cytokines represent the molecular signalling that mediates immune cell communication during active demyelination. The fractional model predicts a cytokine trajectory that is less responsive to sudden changes in therapy, a property with a direct clinical analogue, since cytokine cascades in chronic neuroinflammation typically exhibit substantial persistence despite the initiation of immunomodulatory treatment. The near-equality of the peak amplitudes at $t = 10$ reflects the fact that C_p is a fast variable driven by slower upstream populations; the memory effects redistribute its trajectory in time without dramatically altering its steady-state level.

6.6. Anti-Inflammatory Cytokines (C_a)

Figure 7 compares the integer and fractional dynamics of the anti-inflammatory cytokine field, which conveys the immunosuppressive signal through the model.

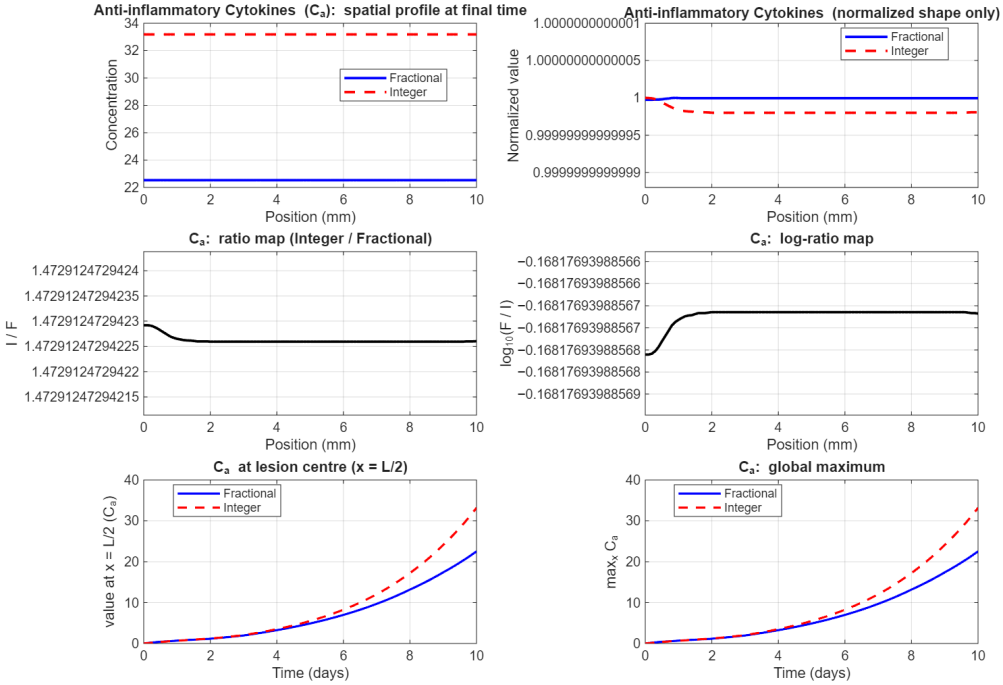

Figure 7. Anti-inflammatory cytokine $C_a(x,t)$ under integer and fractional dynamics. The fractional solution evolves more slowly in time, yielding a reduced final-time amplitude ($C_a^F/C_a^I \approx 0.68$).

6.6.1. Mathematical Interpretation

The C_a population is driven by regulatory T cells (through $\zeta_1 T_r$), M2 macrophages (through $\zeta_2 M_2$) and the therapy source $\xi_6\Phi_1 + \xi_7\Phi_2$. All three sources accumulate more slowly in the fractional formulation, either because they depend on other variables that are themselves delayed (T_r, M_2) or because the therapy source is convolved against the Mittag–Leffler kernel. The compounded effect is visible in Table 2: the fractional peak amplitude is about 32% lower than the integer one, a ratio nearly identical to that of T_r and M_2. This coherent ratio across the regulatory axis (about 0.68 for T_r, M_2, C_a and O) is a signature of the commensurate nature of the memory order across the coupled system.

6.6.2. Biomedical Interpretation

Anti-inflammatory cytokines such as IL-10 and TGF-β orchestrate the resolution of inflammation. Their delayed build-up under fractional dynamics provides a mechanistic explanation for the prolonged active phase of MS lesions observed clinically: even when regulatory signals are being generated, their effective concentration at the lesion site rises more slowly than the inflammatory signals do. This is the molecular-level counterpart of the T_r and M_2 results and reinforces the same qualitative conclusion: memory effects delay the resolution phase more strongly than they delay the activation phase.

6.7. Oligodendrocytes (O) and Demyelinated Area (D)

Figure 8 presents the dynamics of oligodendrocytes, which represent the intact myelin compartment.

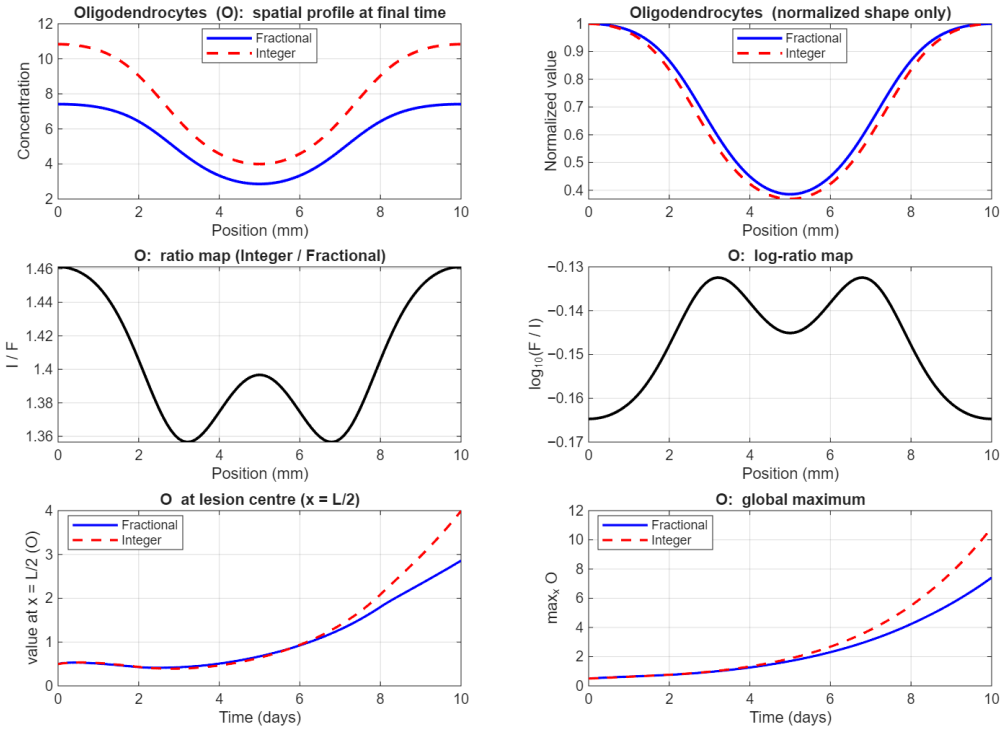

Figure 8. Oligodendrocyte density $O(x,t)$ under integer and fractional dynamics. The fractional solution exhibits a deeper central depletion and a lower global maximum ($O^F/O^I \approx 0.68$), indicating slower reparative recovery.

Figure 9 presents the dynamics of the demyelinated area D(x, t).

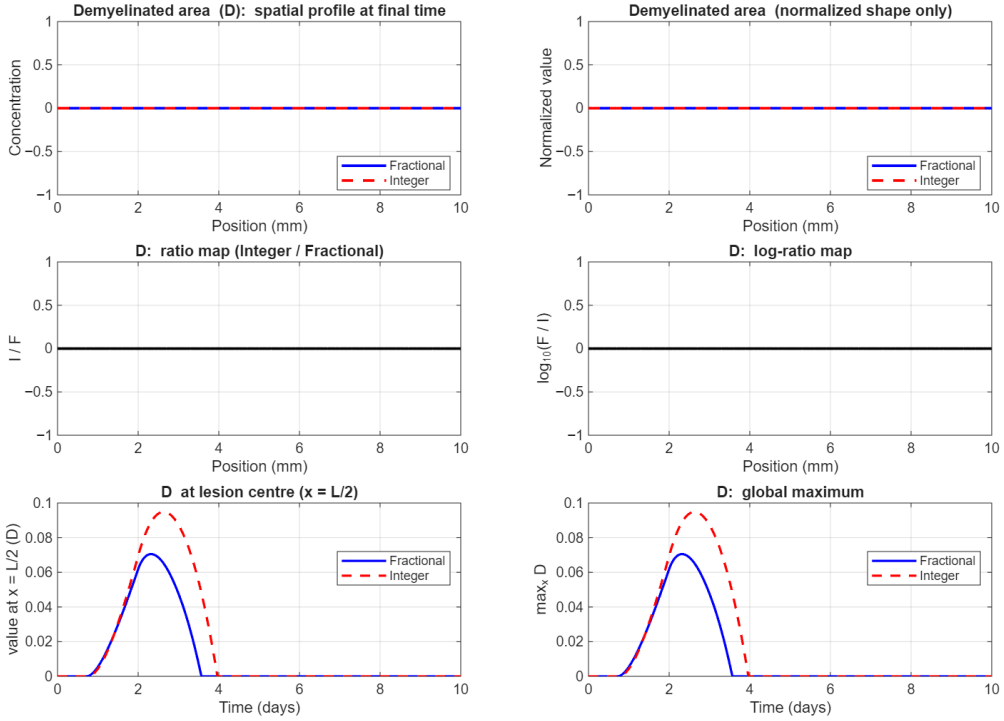

Figure 9. Demyelinated area $D(x,t)$. Over the simulated ten-day window and with the present parameter set, the balance $\lambda_1 C_p O - \lambda_2 M_2$ is non-positive almost everywhere, so that the projected non-negative solution remains at $D = 0$ at the observation time.

6.7.1. Mathematical Interpretation (Oligodendrocytes)

The oligodendrocyte equation combines the cytotoxic loss $-\lambda_1 C_p O$, the reparative source $\lambda_2 M_2$ and the baseline decay $\delta_O O$. Because M_2 is underdeveloped in the fractional formulation, the reparative term is reduced while the cytotoxic term driven by a C_p that is approximately unchanged remains essentially the same. The net effect is a lower oligodendrocyte amplitude ($\max_x O^F \approx 7.4$ versus $\max_x O^I \approx 10.8$, a ratio of 0.68). The spatial profile exhibits a pronounced dip at the lesion centre that is deeper in the fractional case, and the ratio map I/F is close to 1.46 at the periphery while reducing to ≈1.36 at the centre, indicating that the fractional suppression is spatially near-uniform but slightly more pronounced away from the centre.

6.7.2. Mathematical Interpretation (Demyelinated Area)

The demyelinated area equation conserves mass with the oligodendrocyte equation in the sense ${}^{C}D_t^{\alpha}(O + D) = -\delta_O O$. Over the simulated horizon, and with the chosen parameter values, the competition between $\lambda_1 C_p O$ (loss of myelin) and $\lambda_2 M_2$ (remyelination) leaves the net right-hand side of the D equation non-positive, so that the projected non-negative solution remains at $D = 0$ throughout. This is not a failure of the model but rather an indication that on the ten-day horizon and under the specific therapy protocol considered, integrated loss of myelin has not yet exceeded integrated reparative activity. Longer simulation horizons or harsher therapy-absent scenarios would be required to observe the buildup of demyelinated tissue.

6.7.3. Biomedical Interpretation

The reduced oligodendrocyte amplitude in the fractional formulation is the most direct bridge between the mathematical model and the clinical observation of impaired remyelination in progressive MS. The same pro-inflammatory load (C_p approximately unchanged between formulations) is predicted to produce more persistent tissue-level consequences under memory kinetics, because the reparative M2 pathway is slower to mount an effective response. The present simulation, restricted to a ten-day window, captures the early phase of this imbalance; extending the horizon to months or the disease time scale would be expected to reveal progressive accumulation of D that is more severe under the fractional formulation.

6.8. Therapy Protocols

Figure 10 shows the bang–bang therapy functions used in all simulations.

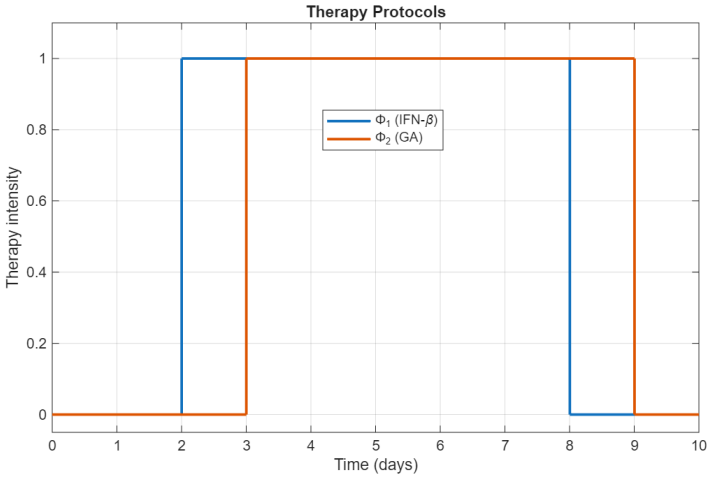

Figure 10. Therapy control functions $\Phi_1(t)$ (IFN-β, active on $[2, 8]$) and $\Phi_2(t)$ (glatiramer acetate, active on $[3, 9]$) used in the simulations. The overlap interval $[3, 8]$ corresponds to combined immunomodulation.

6.8.1. Control-Theoretic Interpretation

The therapy functions enter the governing system multiplicatively (on M_1, T_e, C_p, M_2, T_r and C_a) and therefore act as time-dependent modulators of the corresponding reaction rates. In the integer-order formulation, these inputs modify the instantaneous dynamics, and their effect vanishes as soon as they are switched off. Under the fractional operator, the therapy contribution is convolved against the Mittag–Leffler kernel and therefore continues to influence the solution for $t > 8$ (for IFN-β) and $t > 9$ (for GA), albeit with progressively attenuated weight. The time-series panels for T_e and M_1 (Figures 2 and 4) clearly illustrate this post-therapy persistence: after the therapy switches off, the fractional solution requires additional time to return to the pre-therapy regime, whereas the integer solution recovers immediately.

6.8.2. Biomedical Interpretation

Bang–bang therapy protocols are idealisations of intermittent clinical dosing schedules. The fractional model's prediction of a persistent therapeutic effect beyond the nominal dosing window is biomedically consistent with the pharmacokinetic and pharmacodynamic reality of disease-modifying therapies in MS, in which the biological impact of a given dose extends significantly beyond the period of active drug exposure. This emerges naturally from the CTRW-derived memory structure, without the need for separate pharmacokinetic modelling.

6.9. Overall Assessment

The combined picture emerging from Table 2 and Figures 2–10 can be summarised as follows. The memory-driven fractional dynamics produce a mild amplification of the pro-inflammatory effectors (T_e and M_1, by about 13–15%), an approximate equality of the pro-inflammatory cytokine pool (C_p, ratio ≈ 0.98), and a substantial slowing of the regulatory and reparative variables (T_r, M_2, C_a and O, each reduced by about 32%). The coherence of the latter ratio across four coupled variables is a direct signature of the single commensurate fractional order $\alpha = 0.85$: all variables belong to the same non-Markovian transport process and therefore inherit a shared memory timescale.

This asymmetric pattern effector amplification with regulatory retardation is precisely the kind of mechanistic behaviour that a memory-aware model of MS should exhibit. It provides a natural mathematical correlate of the clinical asymmetry between inflammatory and reparative phases in chronic progressive MS, without requiring heterogeneous fractional orders, additional delay terms, or artificial amplification factors. Importantly, these results are obtained from a dimensionally consistent, mass-conserving formulation that reduces exactly to the classical integer-order model in the Markovian limit $\alpha \to 1$.

We emphasise that the simulation horizon used here ($T = 10$ days) represents the acute phase of lesion evolution. Extension to longer time scales and calibration of the fractional order α and memory timescale τ_0 against longitudinal clinical or imaging data are natural next steps toward quantitative use of the present framework in MS modelling and therapy design.

7. Conclusions

In this study we developed a dimensionally consistent fractional spatio-temporal reaction–diffusion framework for modelling immune-mediated demyelination in multiple sclerosis under IFN-β and glatiramer acetate therapy, integrating adaptive and innate immune responses, cytokine-mediated feedback, macrophage polarisation, oligodendrocyte dynamics, and time-dependent therapeutic modulation within a single distributed-parameter structure. A central methodological feature of the proposed framework is that

the fractional extension is not introduced by ad hoc replacement of integer-order derivatives with Caputo fractional derivatives, an approach that, for coupled reaction–diffusion systems, is known to violate dimensional consistency and mass conservation [26,27]. Instead, we derived the fractional operator from an underlying continuous-time random walk (CTRW) process with Mittag–Leffler-distributed residence times, yielding a governing system in which a single commensurate order $\alpha \in (0, 1]$ and a characteristic memory timescale τ_0 enter through a natural dimensional prefactor τ_0^α. The resulting model is dimensionally consistent, mass-conserving across the coupled components, and reduces exactly to the classical integer-order formulation in the Markovian limit $\alpha \to 1$, $\tau_0 \to 1$ day.

From the mathematical standpoint, we established existence, uniqueness, positivity, boundedness, well-posedness in the sense of Hadamard, and local asymptotic stability of equilibria through a Matignon-type spectral criterion [39], using the fractional Grönwall inequality and Luchko's extremum principle [34] as the main analytical tools. These results confirm that the proposed formulation is both mathematically admissible and biologically sound and provide the rigorous foundation required for subsequent qualitative and numerical analysis. On the computational side, we constructed a structure-preserving IMEX finite-difference scheme in which the stiff diffusive and damping components were treated implicitly while the nonlinear production was handled explicitly. For the fractional case, the Caputo operator was approximated by the classical L1 scheme, and the nonlocal history entered through a weighted sum of past increments without breaking the linearity of the per-step solver. The resulting algorithm is consistent, non-negative under a mild timestep constraint, and recovers the classical integer-order solver in the limit $\alpha \to 1$.

Numerical simulations compared the two formulations over a ten-day horizon under identical parameters, initial data, and bang–bang therapy protocols, so that any difference between the solutions was attributable solely to the non-Markovian residence-time distribution underlying the fractional operator. The results revealed a nuanced and biomedically meaningful pattern rather than a uniform amplification. Pro-inflammatory effectors were moderately elevated under fractional dynamics, the peak amplitudes of T_e and M_1 exceeded their integer-order counterparts by approximately 13–15%, while the pro-inflammatory cytokine pool C_p remained essentially unchanged (ratio $F/I \approx 0.98$). By contrast, the regulatory and reparative variables T_r, M_2, C_a and O all exhibited a coherent reduction, with ratios F/I in the narrow range 0.68–0.69 across four coupled components. This coherence is itself a signature of the commensurate CTRW construction: since all four variables share the same non-Markovian transport process, they inherit a common Mittag–Leffler relaxation timescale and therefore a common retardation factor. Such a consistent pattern cannot be produced by ad hoc fractional replacements with heterogeneous orders and thus constitutes an internal mathematical validation of the dimensionally consistent formulation adopted here.

Biologically, the asymmetry between a mild amplification of the pro-inflammatory arm and a substantial retardation of the regulatory–reparative arm is a faithful mechanistic analogue of chronic progressive MS. In clinical practice, effector populations are often observed to persist despite regulatory responses that mount too slowly to re-establish homeostasis, and reparative M2 polarisation is typically insufficient to keep pace with inflammatory damage. The present fractional model reproduces this imbalance with the same reaction rates that govern the integer-order model, without requiring delay terms, source re-tuning, or heterogeneous fractional orders the imbalance emerges solely from the memory structure inherited from the underlying stochastic process. The therapy simulations carry the same qualitative implication: fractional dynamics predict a persistence of therapeutic influence beyond the nominal dosing window, because the multiplicative control enters the equations through the same memory kernel. This is consistent with the

well-documented pharmacodynamic persistence of disease-modifying therapies in MS and suggests that memory-aware models may naturally capture features that otherwise require separate pharmacokinetic machinery.

Taken together, these results establish that the introduction of temporal memory in a dimensionally consistent manner is not merely a technical correction but a substantive modelling ingredient that reshapes the predicted balance between inflammation, regulation, and repair in MS lesions. The framework is flexible enough to accommodate future refinements including longer simulation horizons, sensitivity analysis with respect to α and τ_0, calibration against longitudinal clinical or imaging data, and extension to higher spatial dimensions or to patient-specific lesion geometries and does so from a foundation that respects the physical and biological requirements of dimensional consistency, mass balance, and positivity. The CTRW-derived fractional formulation therefore provides a principled platform on which memory-aware, mathematically consistent, and biologically interpretable models of immune-mediated neurological diseases can be built, and on which the assessment of therapy protocols for MS can be carried out in a mechanistically transparent way.

Author Contributions: Conceptualization, A.E., M.Y. and F.A.; methodology, A.E. and F.A.; software, A.E.; validation, M.Y., F.A. and F.U.; formal analysis, F.U.; investigation, M.Y., F.A. and F.U.; resources, A.E.; data curation, F.A. M.Y., F.A. and F.U.; visualization, A.E. and M.Y.; supervision, F.A.; project administration, M.Y.; funding acquisition, M.Y. and F.U. All authors have read and agreed to the published version of the manuscript.

Funding: This research received no external funding.

Data Availability Statement: All data generated or analyzed during this study are included in this article.

Acknowledgments: This work was supported by Kyrgyz-Turkish Manas University [Project Number: KTMU-BAP-2026.FB.07].

Conflicts of Interest: The authors declare no conflicts of interest.

References

1. Malakouti, N.; Kessler, D.; Finlayson, M.; Stephens, S. The experience of people with multiple sclerosis who receive occupational performance coaching. *PEC Innov.* **2025**, *7*, 100418. [CrossRef]
2. Walton, C.; King, R.; Rechtman, L.; Kaye, W.; Leray, E.; Marrie, R.A.; Robertson, N.; Rocca, N.L.; Uitdehaag, B.; van der Mei, I.; et al. Rising prevalence of multiple sclerosis worldwide: Insights from the Atlas of MS, third edition. *Mult. Scler. J.* **2020**, *26*, 1816–1821. [CrossRef] [PubMed]
3. Hu, P.; Song, S.; Liu, C.; Xiao, H. A meta-analysis of the effect of computerized cognitive training on cognitive function in patients with multiple sclerosis. *Mult. Scler. Relat. Disord.* **2025**, *104*, 106744. [CrossRef]
4. Gargano, F.; Lombardo, M.C.; Rizzo, R.; Sammartino, M.; Sciacca, V. Cytokine-induced instabilities in a reaction–diffusion-chemotaxis model of Multiple Sclerosis. *Int. J.-Non-Linear Mech.* **2024**, *161*, 104608. [CrossRef]
5. Moghadasi, A.N.; Mirmosayyeb, O.; Bagherieh, S.; Sahraian, M.A.; Ghajarzadeh, M. Computerized cognitive rehabilitation in patients with multiple sclerosis (MS): A systematic review and meta-analysis. *Casp. J. Intern. Med.* **2025**, *16*, 9.
6. Afzal, Z.; Alshehri, M. Error evaluation and stability analysis of numerical schemes in multiple sclerosis modeling. *Ain Shams Eng. J.* **2025**, *16*, 103551. [CrossRef]
7. Zhu, Q.; Li, H.; Wang, R. A conceptual approach to comprehensive interdisciplinary integration in multiple sclerosis modeling. *Front. Comput. Neurosci.* **2025**, *19*, 145–162. [CrossRef]
8. Cheng, Y.; Liu, J.; Tian, F.; Tan, H.; Wang, T.; Lu, J.; Tang, Z.; Ma, X.; Lian, J.; Su, S.; et al. New insight into the mechanism of neurochemical imbalance in multiple sclerosis: Abnormal transportation of brain extracellular space. *Aging Dis.* **2026**, *17*, 452–465. [CrossRef]
9. Aphale, P.; Shekhar, H.; Dokania, S. A critical evaluation of machine learning approaches for screening depression and anxiety in early multiple sclerosis. *Mult. Scler. Relat. Disord.* **2025**, *104*, 106781. [CrossRef]
10. Rehab HQ. *Multiple Sclerosis*; Rehab HQ: Houston, TX, USA, 2021. Available online: https://rehab-hq.com/multiple-sclerosis-2/ (accessed on 2 April 2026).

11. Enver, A.; Ayaz, F.; Yalçınkaya, D.E. A multiscale coupled reaction-diffusion model of amyloid-beta and tau pathology in Alzheimer's disease. *J. Nonlinear Model. Anal.* **2025**, *7*, 1940–1964. [CrossRef]
12. Enver, A.; Ayaz, F. Mathematical modeling of stress-induced type 2 diabetes and atherosclerosis: Numerical methods and stability analysis. *Results Nonlinear Anal.* **2025**, *8*, 204–225. [CrossRef]
13. Enver, A.; Ayaz, F. Melatonin and breast cancer: A mathematical modeling approach in blind women. *Bull. Biomath.* **2025**, *3*, 164–191. [CrossRef]
14. Moise, N.; Friedman, A. A mathematical model of the multiple sclerosis plaque. *J. Theor. Biol.* **2021**, *512*, 110532. [CrossRef]
15. Travaglini, R. A reaction-diffusion model for relapsing-remitting multiple sclerosis with a treatment term. *arXiv* **2024**, arXiv:2407.06802.
16. Oliveira, J.M.; Travaglini, R. Reaction–diffusion systems derived from kinetic theory for Multiple Sclerosis. *Math. Model. Methods Appl. Sci.* **2024**, *34*, 1279–1308. [CrossRef]
17. de Paula, M.A.M.; Quintela, B.d.; Lobosco, M. On the use of a coupled mathematical model for understanding the dynamics of multiple sclerosis. *J. Comput. Appl. Math.* **2023**, *418*, 115163. [CrossRef]
18. Bazlyankov, G.; Ivanov, T. Mathematical modelling of disability progression in patients with multiple sclerosis. *Acta Biotheor.* **2025**, *73*, 7. [CrossRef]
19. Joshi, H.; Yavuz, M. A novel fractional-order model and analysis of cancer-immune system interaction in an avascular environment with an efficient control mechanism. *J. Comput. Appl. Math.* **2026**, *473*, 116888. [CrossRef]
20. Manivel, M.; Venkatesh, A.; Kumawat, S. A comprehensive study of monkeypox disease through fractional mathematical modeling. *Math. Model. Numer. Simul. Appl.* **2025**, *5*, 65–96. [CrossRef]
21. Iwa, L.L.; Omame, A.; Inyama, S.C. A fractional-order model of COVID-19 and Malaria co-infection. *Bull. Biomath.* **2024**, *2*, 133–161. [CrossRef]
22. Nisar, K.S.; Farman, M. A review on fuzzy fractional order modeling in health systems with application to cardiovascular disease. *Int. J. Math. Comput. Eng.* **2026**, *4*, 235–260. [CrossRef]
23. Ata, E.; Kıymaz, I.O. Special functions with general kernel: Properties and applications to fractional partial differential equations. *Int. J. Math. Comput. Eng.* **2025**, *3*, 153–170. [CrossRef]
24. Hızalı, Ş.F.; Alsindi, B.J.K.; Agamalieva, L.; Bulut, H. Caputo fractional derivative applied to transmission dynamics of monkeypox virus. *Adv. Math. Model. Appl.* **2025**, *10*, 627–647. [CrossRef]
25. Jafari, H.; Tajadodi, H.; Gasimov, Y.S. *Modern Computational Methods for Fractional Differential Equations*; Taylor & Francis: Boca Raton, FL, USA, 2025. [CrossRef]
26. Angstmann, C.N.; Henry, B.I. Time fractional Fisher–KPP and FitzHugh–Nagumo equations. *Entropy* **2020**, *22*, 1035. [CrossRef]
27. Angstmann, C.N.; Erickson, A.M.; Henry, B.I.; McGann, A.V.; Murray, J.M.; Nichols, J.A. A general framework for fractional order compartment models. *SIAM Rev.* **2021**, *63*, 375–392. [CrossRef]
28. Angstmann, C.N.; Henry, B.I.; McGann, A.V. A fractional order recovery SIR model from a stochastic process. *Bull. Math. Biol.* **2016**, *78*, 468–499. [CrossRef]
29. Lombardo, M.C.; Barresi, R.; Bilotta, E.; Gargano, F.; Pantano, P.; Sammartino, M. Demyelination patterns in a mathematical model of multiple sclerosis. *J. Math. Biol.* **2017**, *75*, 373–417. [CrossRef]
30. Marino, S.; Hogue, I.B.; Ray, C.J.; Kirschner, D.E. A methodology for performing global uncertainty and sensitivity analysis in systems biology. *J. Theor. Biol.* **2008**, *254*, 178–196. [CrossRef] [PubMed]
31. Maiti, S.; Dai, W.; Alaniz, R.C.; Hahn, J.; Jayaraman, A. Mathematical modeling of pro- and anti-inflammatory signaling in macrophages. *Processes* **2015**, *3*, 1–18. [CrossRef]
32. Torres, M.; Wang, J.; Yannie, P.J.; Ghosh, S.; Segal, R.A.; Reynolds, A.M. Identifying important parameters in the inflammatory process with a mathematical model of immune cell influx and macrophage polarization. *PLoS Comput. Biol.* **2019**, *15*, e1007172. [CrossRef] [PubMed]
33. Kumar, R.; Clermont, G.; Vodovotz, Y.; Chow, C.C. The dynamics of acute inflammation. *J. Theor. Biol.* **2004**, *230*, 145–155. [CrossRef] [PubMed]
34. Luchko, Y. Maximum principle for the generalized time-fractional diffusion equation. *J. Math. Anal. Appl.* **2009**, *351*, 218–223. [CrossRef]
35. Arbogast, T.; Bona, J.L. *Functional Analysis for the Applied Mathematician*; Textbooks in Mathematics; CRC Press (Taylor & Francis Group): Boca Raton, FL, USA, 2025. [CrossRef]
36. Papageorgiou, N.S.; Winkert, P. *Applied Nonlinear Functional Analysis: An Introduction*; De Gruyter Textbook: Berlin, Germany, 2024; ISBN 978-3-11-132874-5.
37. Brezis, H. *Functional Analysis, Sobolev Spaces and Partial Differential Equations*; Universitext; Springer: New York, NY, USA, 2011. [CrossRef]

38. Lee, J.M. *Introduction to Smooth Manifolds*; Graduate Texts in Mathematics; Springer: New York, NY, USA, 2003; Volume 218. [CrossRef]
39. Matignon, D. Stability results for fractional differential equations with applications to control processing. In Proceedings of the Computational Engineering in Systems Applications (IMACS, IEEE-SMC), Lille, France, 9–12 July 1996; Volume 2, pp. 963–968.